Article

Cell Reports

Experience-Dependent Development and Maintenance of Binocular Neurons in the Mouse Visual Cortex

Graphical Abstract

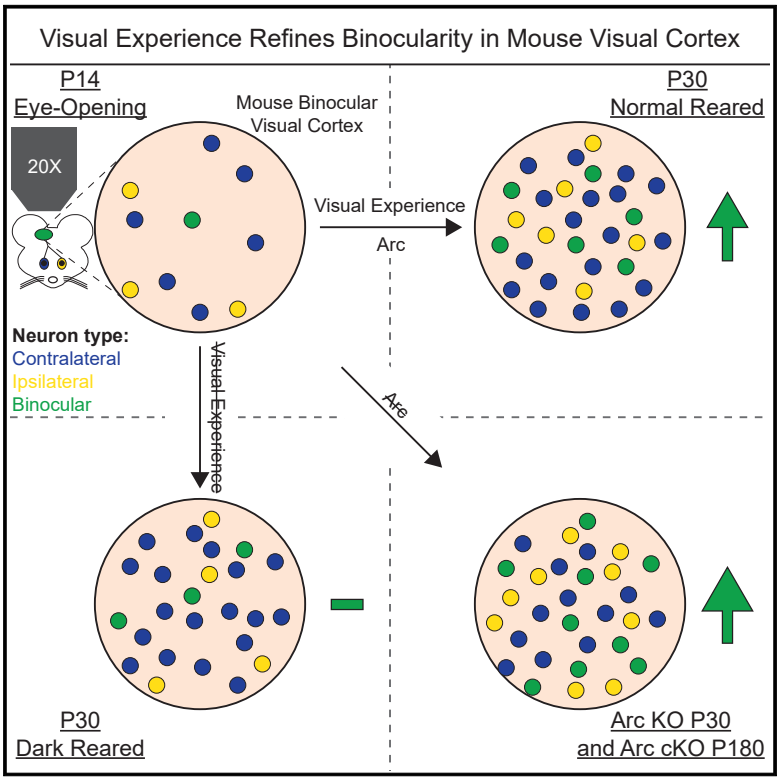

Highlights

- Binocular neurons in mouse V1 develop after eye-opening by visual experience
- Binocular neurons acquire distinct visual response properties
- The neuronal gene Arc limits the development of binocular neurons
- Arc-dependent plasticity maintains binocularity even in adult V1

Authors

Kyle R. Jenks, Jason D. Shepherd

Correspondence

jason.shepherd@neuro.utah.edu

In Brief

Jenks and Shepherd show that neurons responding to both eyes in the mouse visual cortex develop with experience. These binocular neurons acquire unique visual response properties, such as a preference for horizontal orientations. The neuronal gene Arc limits and maintains the number of binocular neurons, even in the adult cortex.

Jenks & Shepherd, 2020, Cell Reports *30*, 1982–1994
February 11, 2020
https://doi.org/10.1016/j.celrep.2020.01.031

CellPress

OPEN ACCESS
CellPress

Cell Reports
Article

Experience-Dependent Development and Maintenance of Binocular Neurons in the Mouse Visual Cortex

Kyle R. Jenks[1] and Jason D. Shepherd[1,2,3,*]
[1]Department of Neurobiology and Anatomy, The University of Utah, Salt Lake City, Utah 84112, USA
[2]Department of Ophthalmology and Visual Sciences, The University of Utah, Salt Lake City, Utah 84112, USA
[3]Lead Contact
*Correspondence: jason.shepherd@neuro.utah.edu
https://doi.org/10.1016/j.celrep.2020.01.031

SUMMARY

The development of neuronal circuits requires both hard-wired gene expression and experience-dependent plasticity. Sensory processing, such as binocular vision, is especially sensitive to perturbations of experience. We investigated the experience-dependent development of the binocular visual cortex at single-cell resolution by using two-photon calcium imaging in awake mice. At eye-opening, the majority of visually responsive neurons are monocular. Binocular neurons emerge later with visual experience and acquire distinct visual response properties. Surprisingly, rather than mirroring the effects of visual deprivation, mice that lack the plasticity gene *Arc* show increased numbers of binocular neurons and a shift in ocular dominance during development. Strikingly, acutely removing *Arc* in the adult binocular visual cortex also increases the number of binocular neurons, suggesting that the maintenance of binocular circuits requires ongoing plasticity. Thus, experience-dependent plasticity is critical for the development and maintenance of circuits required to process binocular vision.

INTRODUCTION

Sensory processing requires the development of neuronal circuits that can reliably encode information from the environment and adapt to novel sensory experience. Thus, the shaping of brain circuits requires both hard-wired patterning and experience-dependent plasticity. Experience-dependent processes predominately occur early in development during critical periods of heightened plasticity. This is particularly evident in the primary visual cortex (V1), where manipulation of visual experience early in life can lead to dramatic changes in function and structure (Espinosa and Stryker, 2012). Closing one eye for several days during this critical period drives the loss of input from the deprived eye in binocular V1, resulting in a shift in ocular dominance (OD). Although the mechanisms of OD plasticity are well studied (Levelt and Hübener, 2012), it remains unclear whether similar mechanisms mediate the normal development of visual response properties in binocular V1.

V1 receives visual input from both eyes and needs to integrate this information to resolve an accurate representation of visual space. In cats and most primates, eye-specific input into V1 form alternating OD columns, as well as orientation columns arranged in pinwheels, which are dominated by the contralateral eye early in development (Crair et al., 1998; Hubel et al., 1976). This structural organization seems to arise independent of visual experience, although other visual response properties and the strengthening of ipsilateral input require experience (Crair et al., 1998; Li et al., 2006; Rakic, 1976; Sherk and Stryker, 1976). Mice lack distinct OD columns (Dräger, 1975). However, neurons within mouse binocular V1 still display a range of OD bias and orientation selectivity (Figueroa Velez et al., 2017; Salinas et al., 2017; Smith and Trachtenberg, 2007). Recent studies have also shown that orientation selectivity between neighboring neurons correlates as a function of cortical distance and cortical depth, consistent with a primitive columnar organization (Ringach et al., 2016). Studies using intrinsic imaging in mouse V1 suggest that eye-specific plasticity begins at eye-opening, especially in the establishment of ipsilateral eye connectivity (Smith and Trachtenberg, 2007). The contralateral eye drives the majority of initial input into V1, and the refinement and strengthening of ipsilateral eye responsiveness require patterned contralateral visual input, although it is unclear how this large-scale refinement of ipsilateral input relates to the integration of binocular input at the level of single neurons.

One important function of binocular V1 refinement is to match specific visual responses from each eye onto binocular neurons. Initially, these inputs respond to different orientations but become matched during the critical period (Wang et al., 2010). This binocular matching requires visual experience and NMDA receptor activity (Wang et al., 2010, 2013). These mechanisms resemble those of OD plasticity, and monocular deprivation can disrupt binocular matching (Levine et al., 2017). In monocular V1, using electrophysiological recordings, researchers have obsered layer-specific maturation of orientation and direction selectivity rapidly after eye-opening (Hoy and Niell, 2015). Dark rearing or genetically reducing neuronal activity in monocular V1 has little effect on the initial formation of orientation and direction selectivity (Hagihara et al., 2015; Rochefort et al., 2011). Although experience does not seem to be critical for monocular V1 development, it remains unclear whether these

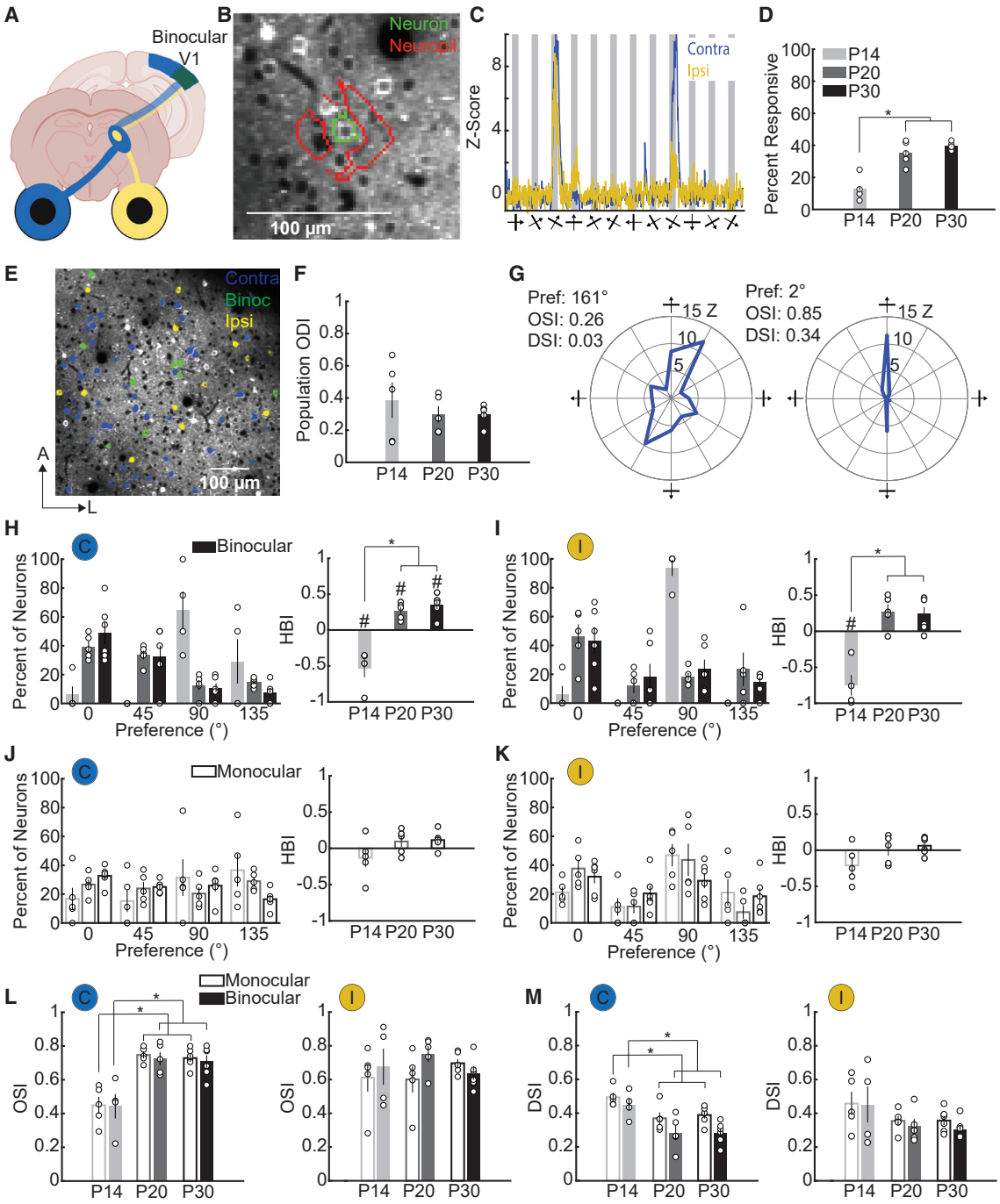

Figure 1. Visual Response Properties in L2/3 Excitatory Neurons of Binocular V1 Are Rapidly Tuned after Eye-Opening

(A) Imaging was performed in mouse binocular V1.

(B) ROIs corresponding to the soma of a neuron (green outline) and the surrounding area of neuropil (red outline).

(C) The averaged responses of an example neuron to stimuli (gray bars = stimuli presentation) through the contralateral (blue) and ipsilateral (yellow) eye, after neuropil subtraction and *Z* scoring. The orientation and direction (arrow) of each stimulus is indicated below the x axis.

(D) Percentage of neurons that are visually responsive at each time point.

(E) Representative image of L2/3 excitatory neuron recordings, showing contralateral (contra, blue), ipsilateral (ipsi, yellow), and binocular (binoc, green) neurons.

(F) ODI of the total population of visually responsive neurons. An ODI of 0 is purely contralateral and 1 purely ipsilateral.

(G) Example tuning curves for two neurons showing orientation preference (Pref), OSI, and DSI.

(H) Distribution of orientation preference in binocular neurons for contralateral responses at each age and HBI.

(I) Distribution of orientation preference in binocular neurons for ipsilateral response and HBI.

(legend continued on next page)

findings also generalize to binocular V1. Given the role of experience in the development of OD and binocular matching in binocular V1 during the critical period, distinct processes may govern the development of monocular and binocular V1.

Molecular mechanisms reminiscent of cellular models of plasticity, such as long-term potentiation and depression (LTP/LTD), mediate OD plasticity (Yoon et al., 2009). However, little is known about the contribution of these mechanisms to the development and refinement of visual response properties. Visual experience induces expression of the immediate-early gene *Arc* in excitatory neurons of the visual cortex (Tagawa et al., 2005). *Arc* is necessary for OD plasticity and LTD in binocular V1 (Jenks et al., 2017; McCurry et al., 2010). The induction of Arc expression declines past the close of the critical period, and increasing Arc expression in the adult brain can restore juvenile-like OD plasticity (Jenks et al., 2017). Thus, Arc may also have a role in the experience-dependent development of binocular visual response properties.

To determine how visual response properties develop in binocular V1, we used two-photon *in vivo* calcium imaging to examine the visual response properties of individual neurons at various points after eye-opening. To determine the contribution of experience and synaptic plasticity, we also imaged dark-reared (DR) mice and Arc knockout (KO) mice. Finally, we examined whether Arc's role in vision is confined to development by knocking out Arc in adult binocular V1.

RESULTS

Visually Responsive Neurons Emerge after Eye-Opening

To measure visual response properties of single neurons, we conducted acute, two-photon calcium imaging through cranial windows implanted over binocular V1 (Figure 1A) in cohorts of mice expressing GCaMP6s driven by the Thy1 promoter, which labels the majority of excitatory neurons in layer (L) 2/3 (Dana et al., 2014; Feng et al., 2000; Lee et al., 2017; Sun et al., 2016). To capture the development of response properties after eye-opening, we imaged at three time points in separate cohorts of mice: postnatal day 14 (P14) corresponding to 0–2 days after eye-opening, P20 immediately before the start of the canonical OD plasticity critical period, and P30, the peak of the OD critical period. We determined the location of binocular V1 stereotaxically (see STAR Methods). To confirm that stereotaxic coordinates in P14 mice reliably target V1, we conducted chronic retinotopic mapping at P14 and P20 (Figures S1A–S1C). We found that the retinotopy/V1 location was consistent from P14 to P20 and the boundary of the imaging window did not overlap with areas of phase reversal that would signal the transition into a secondary visual area (Murakami et al., 2017; Zhuang et al., 2017). These results confirm that our P14 two-photon recordings accurately depict V1 responses.

For two-photon imaging, we presented visual stimuli in the form of drifting, sinusoidal gratings with orientations (0–330°) in 30° increments at 0.05 cycles/degree (previously shown to maximally stimulate V1; Gu et al., 2013; Hoy and Niell, 2015; Niell and Stryker, 2008), interleaved with gray screen presentations. Regions of interest (ROIs) corresponding to neuronal soma were selected automatically and manually annotated (see STAR Methods). We subtracted the neuropil fluorescence around the soma (Peron et al., 2015) to remove contaminating signals from surrounding processes (Figure 1B). Visually evoked neuronal activity was quantified using a Z score as previously described (El-Boustani et al., 2018; Figure 1C). Spontaneous activity during the gray screen periods did not significantly differ across age (Figure S2A; P14 = 0.66 ± 0.07 (ΔF/F)/S, P20 = 0.61 ± 0.02 (ΔF/F)/S, P30 = 0.56 ± 0.04 (ΔF/F)/S, $F_{2,13}$ = 1.1, p = 0.3758, ANOVA). However, the percent of visually responsive neurons increased significantly from 13% ± 3% (mean ± standard error of the group) at P14 to 40% ± 1% in P30 wild-type (WT) mice (Figure 1D; P14 = 27 ± 7 total responsive neurons/mouse, n = 5; P20 = 59 ± 7 neurons/mouse, n = 5; P30 = 60 ± 3 neurons/mouse, n = 6; $F_{2,13}$ = 30.8, p < 0.0001, ANOVA). To verify that 0.05 cycles/degree maximally stimulates visual responses, in a separate cohort of P30 mice, we presented a range of spatial frequencies. We found no significant difference in the percent of visually responsive neurons compared with using 0.05 cycles/degree alone (Figure S2B; 0.025–0.4 = 50 ± 6%, $F_{1,9}$ = 3.2, p = 0.1062, ANOVA). Because long imaging sessions in awake animals can lead to spurious results, we used 0.05 cycles/degree in all subsequent experiments.

Visually responsive neurons were further classified as either binocularly responsive, where the neuron showed significant visual responses to stimulation of both the contralateral and ipsilateral eye independently, or monocularly responsive if the neurons responded solely to either the contralateral eye or ipsilateral eye (Figure 1E). The spatial distribution of binocular and ipsilateral responses appeared widely dispersed across the field of view, discounting the possibility that our recordings were in or near the boundary of monocular V1. We quantified the OD index (ODI) of neurons on a scale of 0 (purely contralateral responsive) to 1 (purely ipsilateral responsive) and averaged all neurons recorded per mouse before averaging within each age group (Figure 1F). The ODI of the population did not vary across age groups (P14 = 0.39 ± 0.11, P20 = 0.30 ± 0.05, P30 = 0.30 ± 0.02; $F_{2,13}$ = 0.6, p = 0.5888, ANOVA).

Distinct Development of Response Properties in Binocular Neurons

To determine how visual response properties develop in binocular V1, we quantified orientation preference, orientation

(J) Distribution of orientation preference and HBI for contralateral monocular neurons.
(K) Distribution of orientation preference and HBI for ipsilateral monocular neurons.
(L) Quantification of OSI.
(M) Quantification of DSI (*p < 0.05 indicates a significant difference between groups; #p < 0.05 indicates a significant difference within a group from the expected mean; error bars represent standard error of the mean; open circles indicate a data point from an individual mouse; n = number of animals for all statistics).
See also Figures S1 and S2.

selectivity, and direction selectivity across age, as these properties are important for visual feature detection (Figure 1G). We analyzed the eye-specific responses in binocular and monocular neurons separately. In P14 mice, the few binocular responsive neurons preferred vertical orientations (90°), whereas in P20 and P30 mice, binocular neurons preferred horizontal (0°) orientations (Figures 1H and 1I). To quantify the degree of bias for cardinal orientations, we measured the horizontal bias index (HBI) of neurons, which ranks the bias of neurons from −1 (vertical) to 1 (horizontal), with 0 representing no cardinal bias (Figure 1H; Hagihara et al., 2015). Contralateral responses of binocular neurons in P14 mice had a significant bias for vertical orientations (P14 = −0.53 ± 0.14, t = −3.8, p = 0.0326, t test), whereas P20 and P30 mice had a significant bias for horizontal orientations (P20 = 0.27 ± 0.05, t = 5.2, p = 0.0066; P30 = 0.35 ± 0.06, t = 5.9, p = 0.0020, t test). Contralateral HBI of binocular neurons was significantly different between P14 mice and P20/P30 mice ($F_{2,12}$ = 31.8, p < 0.0001, ANOVA). Ipsilateral responses of binocular neurons had a similar bias for vertical orientations at P14 (Figure 1I; P14 HBI: −0.75 ± 0.16, t = −4.7, p = 0.0184, t test) and also had a shift toward horizontal orientations in P20/30 animals ($F_{2,12}$ = 22.5, p < 0.0001, ANOVA). Interestingly, monocular neurons had no vertical bias at P14 and did not switch to a horizontal bias during development in either contralateral or ipsilateral responsive neurons (Figures 1J and 1K). Thus, a developmental switch in orientation bias occurs only in binocular neurons.

We next measured the orientation selectivity of neurons, quantified as an orientation selectivity index (OSI) (see STAR Methods). Both monocular and binocular neuron OSI to the contralateral eye increased significantly from P14 to P20 and P30 (Figure 1L; contralateral monocular: P14 = 0.45 ± 0.05, P20 = 0.75 ± 0.02, P30 = 0.73 ± 0.02, $F_{2,13}$ = 25.1, p < 0.0001, ANOVA; contralateral binocular: P14 = 0.44 ± 0.08, P20 = 0.72 ± 0.04, P30 = 0.71 ± 0.04, $F_{2,12}$ = 8.7, p = 0.0047, ANOVA). In contrast, OSI to the ipsilateral eye did not significantly change with age in monocular and binocular neurons (Figure 1L; ipsilateral monocular: P14 = 0.61 ± 0.09, P20 = 0.60 ± 0.08, P30 = 0.70 ± 0.02, $F_{2,13}$ = 0.7, p = 0.5154, ANOVA; ipsilateral binocular: P14 = 0.68 ± 0.12, P20 = 0.75 ± 0.05, P30 = 0.63 ± 0.04, $F_{2,12}$ = 0.9, p = 0.4390, ANOVA). This suggests that OSI tuning develops specifically in contralateral eye inputs. The direction selectivity index (DSI) was calculated for all neurons (see STAR Methods). Both monocular and binocular neuron DSI to the contralateral eye decreased significantly over age (Figure 1M; contralateral monocular: P14 = 0.50 ± 0.03, P20 = 0.37 ± 0.03, P30 = 0.39 ± 0.02, $F_{2,13}$ = 5.9, p = 0.0152, ANOVA; contralateral binocular: P14 = 0.45 ± 0.04, P20 = 0.28 ± 0.04, P30 = 0.28 ± 0.03, $F_{2,12}$ = 6.0, p = 0.0157, ANOVA), whereas DSI to the ipsilateral eye was unchanged (Figure 1M; ipsilateral monocular: P14 = 0.46 ± 0.07, P20 = 0.35 ± 0.03, P30 = 0.36 ± 0.03, $F_{2,13}$ = 1.7, p = 0.2253, ANOVA; ipsilateral binocular: P14 = 0.45 ± 0.12, P20 = 0.32 ± 0.04, P30 = 0.30 ± 0.02, $F_{2,12}$ = 1.5, p = 0.2534, ANOVA). Thus, similar to OSI, developmental tuning of DSI occurs specifically in contralateral inputs. A broader range of spatial frequencies in a separate cohort of P30 mice did not significantly change measured contralateral OSI or DSI (Figure S2C: 0.025–0.4 OSI = 0.63 ± 0.07, $F_{1,9}$ = 1.1, p = 0.3204, ANOVA; Figure S2D: 0.025–0.4 DSI = 0.37 ± 0.03, $F_{1,9}$ = 4.7, p = 0.0591, ANOVA).

These results reflect the complex developmental fine tuning of visual response properties in binocular V1. Interestingly, the tuning of visual responses did not change significantly from P20 to P30, suggesting many aspects of visual development in binocular V1 mature before the start of the classical OD critical period in mice. Tuning of visual response properties occurs mostly through contralateral eye input, and binocular neurons become uniquely biased toward horizontal orientations, indicating that these neurons may mediate distinct processing of visual information.

The Development of Binocular Neurons Requires Visual Experience

Our results suggest that binocular neurons have specific visual response properties that differ from monocular neurons; therefore, we investigated these binocular neurons in more detail. Only a small percentage of visually responsive cells were binocular at P14, with most cells responding only to the contralateral or ipsilateral eye (Figures 2A and 2B). However, the percentage of binocular cells significantly increased with age (Figure 2B; P14 = 8% ± 3%, P20 = 25% ± 3%, P30 = 17% ± 2%, $F_{2,13}$ = 9.0, p = 0.0036, ANOVA). This increase was not due to more neurons becoming visually responsive, as the probability of a visually responsive neuron being binocular by chance does not change over age (Figure S2E; P14 = 0.20 ± 0.03, P20 = 0.22 ± 0.01, P30 = 0.22 ± 0.01, $F_{2,13}$ = 0.6, p = 0.5456, ANOVA). A broader range of spatial frequencies in a separate cohort of P30 mice did not significantly change the percent of visually responsive neurons that were binocular compared to P30 mice stimulated with 0.05 cycles/degree (Figure S2F; 0.025–0.4 = 24% ± 5%, $F_{1,9}$ = 1.9, p = 0.1998, ANOVA). We also assessed the relative strength of contralateral and ipsilateral inputs to binocular neurons. The ODI of binocular neurons did not change over age (Figure 2C; P14 = 0.39 ± 0.08, P20 = 0.45 ± 0.04, P30 = 0.38 ± 0.03, $F_{2,12}$ = 0.5, p = 0.6229, ANOVA). These findings suggest that binocularity in L2/3 neurons in mouse V1 is initially represented at the population level by monocularly driven cells, whereas individual cells become binocularly responsive later in development.

Previous studies have reported a large mismatch in orientation preference between the two eyes in binocular V1 neurons (averaged across layers) early in development (Wang et al., 2010, 2013). We examined binocular matching of orientation preference across age in L2/3 neurons, measured as the binocular offset between the orientation preference of the contralateral and ipsilateral responses in binocular neurons. We found that in L2/3 neurons the mean binocular offset was low for all ages examined and did not change across age (Figure S2G; P14 = 19.3 ± 4.4°, P20 = 22.6 ± 3.7°, P30 = 23.6 ± 2.4°, $F_{2,12}$ = 0.4, p = 0.6826, ANOVA).

The contribution of visual experience to the maturation of visual responses in binocular V1 is unclear. To determine the contribution of visual experience, we DR mice from birth in complete darkness until P30, with controls raised on a normal 12:12-h light-dark cycle (normally reared [NR]). NR and DR mice did not differ in the total percentage of neurons that were visually responsive (Figure 2D; NR = 41 ± 4 neurons/mouse, n = 7, 33.2% ± 8.4%;

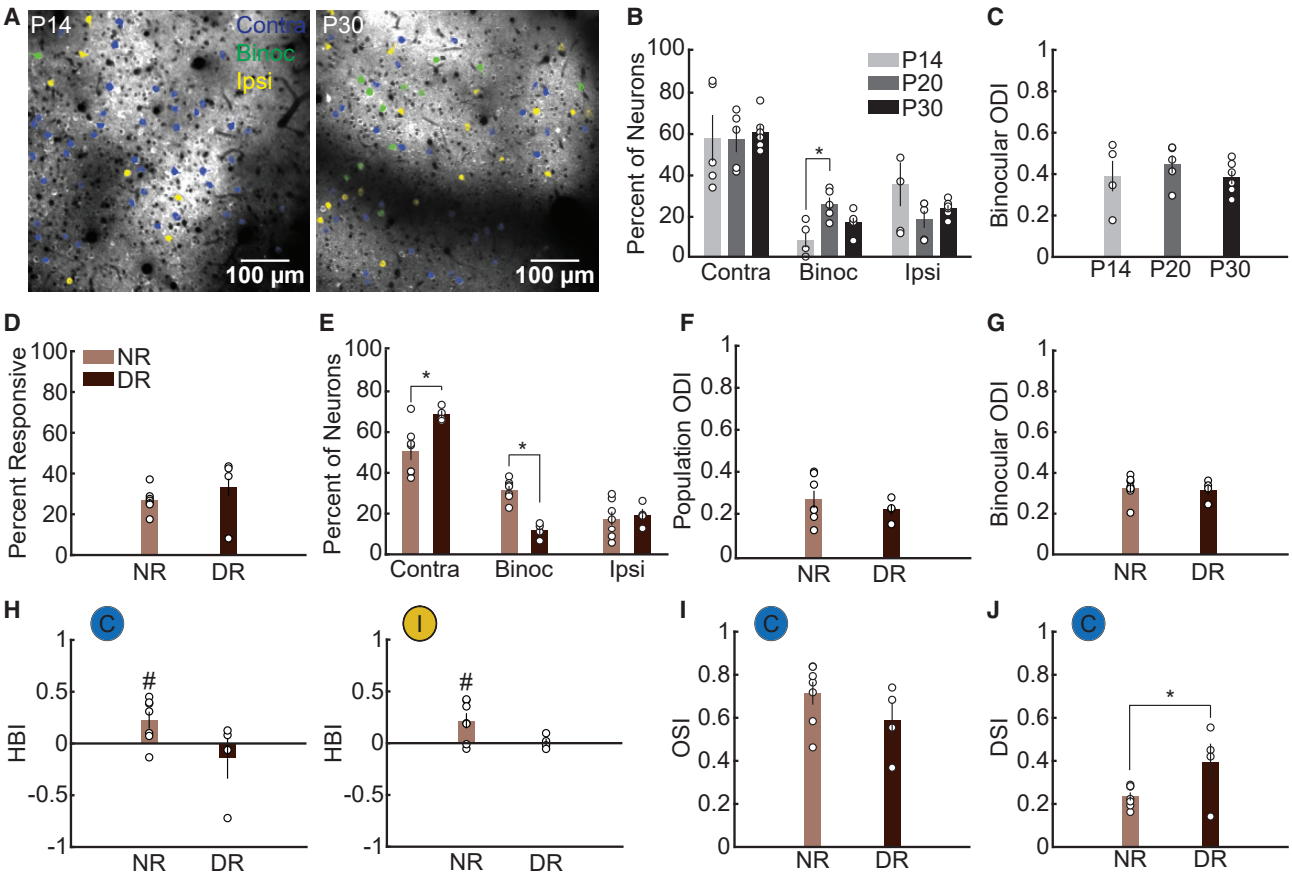

Figure 2. Experience-Dependent Development of Binocular Neurons

(A) Representative images from two-photon recording of visually evoked calcium responses.

(B) Percentage of visually responsive neurons that are monocular or binocular across age.

(C) ODI of binocular neurons across development.

(D) Percentage of neurons responsive to visual stimulation in normally reared (NR) and dark-reared (DR) mice.

(E) Percentage of visually responsive neurons that are monocular or binocular in NR and DR mice.

(F) ODI of the total visually responsive neuron population in NR and DR mice.

(G) ODI of binocular neurons in NR and DR mice.

(H) HBI of binocular neurons in NR and DR mice.

(I) Contralateral OSI of binocular neurons in NR and DR mice.

(J) Contralateral DSI of binocular neurons in NR and DR mice (*$p < 0.05$ indicates a significant difference between groups; #$p < 0.05$ indicates a significant difference within a group from the expected mean; error bars represent standard error of the mean; open circles indicate a data point from an individual mouse; n = number of animals for all statistics).

See also Figure S2.

DR = 67 ± 18 neurons/mouse n = 4, 26.5% ± 2.2%, $F_{1,9} = 1.0$, $p = 0.3463$, ANOVA). We examined the distribution of binocular neurons within the population of responsive neurons (Figure 2E). At P30, DR mice had significantly more monocular contralateral neurons (Figure 2E; NR = 50.8% ± 4.6%, DR = 68.8% ± 1.7%, $F_{1,9} = 8.1$, $p = 0.0191$, ANOVA) and significantly fewer binocular neurons (NR = 31.7% ± 1.9%, DR = 11.7% ± 1.9%, $F_{1,9} = 46.1$, $p < 0.0001$, ANOVA) than NR mice, reminiscent of P14 NR animals (Figure 2B). Despite the change in the number of visually responsive neurons that were binocular versus monocular, the ODI of the total population of neurons was not different (Figure 2F; NR = 0.28 ± 0.04, DR = 0.23 ± 0.03, $F_{1,9} = 0.7$, $p = 0.4285$, ANOVA). Additionally, the ODI of binocular neurons did not differ between NR and DR mice (Figure 2G; NR = 0.33 ± 0.02, DR = 0.32 ± 0.03, $F_{1,9} = 0.1$, $p = 0.7977$, ANOVA). We also did not observe a significant difference in binocular offset between NR and DR mice, although there was a trend toward higher offsets in DR mice (Figure S2H; NR = 20.4 ± 2.6°, DR = 33.7 ± 7.4°, $F_{1,9} = 4.3$, $p = 0.0683$, ANOVA). These findings indicate that visual experience is crucial to the emergence of binocular neurons.

We measured orientation preference, OSI, and DSI in NR and DR binocular neurons to see if these response properties are tuned by experience. Binocular neurons in NR mice show a

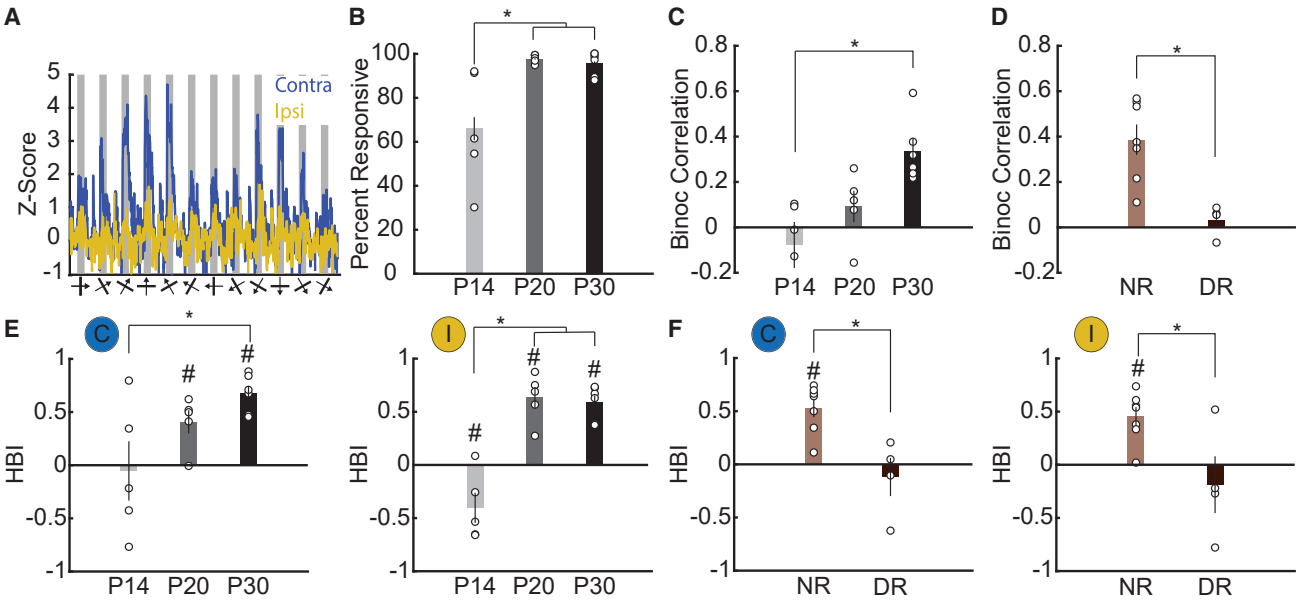

Figure 3. Visual Experience Drives Correlated Binocular Activity in the Neuropil during Development

(A) Example calcium responses of a binocular region of neuropil to the contralateral (blue trace) and ipsilateral (yellow trace) eye.

(B) Percentage of neurons with surrounding neuropil that respond to visual stimuli.

(C) Signal correlation of contralateral and ipsilateral activity in binocular neuropil.

(D) Binocular signal correlation in DR mice.

(E) HBI of the responses in binocular neuropil across age.

(F) HBI of the responses in binocular neuropil of NR and DR mice (*$p < 0.05$ indicates a significant difference between groups; #$p < 0.05$ indicates a significant difference within a group from the expected mean; error bars represent standard error of the mean; open circles indicate a data point from an individual mouse; n = number of animals for all statistics).

bias to horizontal orientations for contralateral and ipsilateral responses (Figure 2H; NR contralateral HBI = 0.23 ± 0.08, t = 2.8, p = 0.0327; ipsilateral NR HBI = 0.22 ± 0.07, t = 2.9, p = 0.0262, t test), similar to the results in P30 WT mice. Neither the contralateral (DR HBI = −0.14 ± 0.20, t = −0.7, p = 0.5161, t test) or ipsilateral (DR HBI = 0.01 ± 0.03, t = 0.31, p = 0.7775, t test) responses in binocular neurons in DR mice showed a significant bias, although the difference between NR and DR mice is not significant (contralateral: $F_{1,9} = 4.2$, p = 0.0702; ipsilateral: $F_{1,9} = 4.0$, p = 0.0755, ANOVA). The contralateral OSI in binocular neurons was not significantly different between NR and DR mice (Figure 2I; NR = 0.71 ± 0.05, DR = 0.59 ± 0.08, $F_{1,9} = 1.8$, p = 0.2074, ANOVA). The mean contralateral DSI of binocular neurons, however, was significantly lower in NR mice than DR mice, indicating the developmental decrease in DSI is experience dependent (Figure 2J; NR = 0.23 ± 0.02, DR = 0.39 ± 0.09, $F_{1,9} = 5.2$, p = 0.0485, ANOVA). These results show that, except for OSI, fine tuning of visual response properties in binocular neurons requires visual experience.

Visual Experience Drives Correlated Binocular Activity in the Neuropil

The neuropil is comprised of intracortical axons and dendrites from L2/3, L4, and L5, as well as thalamic projections into V1. Thy1 GCaMP6s mice express a high density of GCaMP6s in the neuropil (Dana et al., 2014). Do neuropil responses show any developmental-dependent tuning in visual responses or binocularity? We examined visual responses of neuropil patches taken as an annulus around the soma of all detected neurons (see STAR Methods) and found that many patches displayed significant visual responses evoked by either eye (Figure 3A). Similar to neurons, the percentage of neuropil patches with significant visual responses increased over age (Figure 3B; P14 = 66% ± 11.7%, P20 = 97.8% ± 0.9%, P30 = 95.5% ± 2.2%, $F_{2,13} = 7.2$, p = 0.0079, ANOVA). Because binocular neurons only emerge after eye-opening, we predicted that correlated binocular tuning in the neuropil would also emerge after eye-opening. To test this, we measured the signal correlation between mean contralateral and ipsilateral responses in binocular neuropil (Jeon et al., 2018; Ko et al., 2013). The correlation of the contralateral and ipsilateral responses was extremely low at P14 and P20 but increased significantly at P30 (Figure 3C; P14 = −0.08 ± 0.1, P20 = 0.09 ± 0.07, P30 = 0.33 ± 0.06, $F_{2,13} = 7.8$, p = 0.0060, ANOVA). We next examined whether this increase in correlated activity between the eyes over development is experience dependent. Correlation between contralateral and ipsilateral responses in neuropil patches was 0.39 ± 0.07 in NR mice but was absent in DR mice at 0.03 ± 0.03 (Figure 3D; $F_{1,9} = 14.0$, p = 0.0046, ANOVA).

We next examined orientation preference of neuropil patches across development to determine whether neuropil orientation preference showed similar biases to binocular neurons. At P14, an orientation bias for vertical orientations is present for the ipsilateral but not the contralateral eye (Figure 3E;

contralateral = −0.05 ± 0.28, t = −0.2, p = 0.8564; ipsilateral = −0.40 ± 0.14, t = −2.8, p = 0.0470, t test). However, P20 (Figure 3E; contralateral = 0.41 ± 0.11, t = 3.7, p = 0.0200; ipsilateral = 0.63 ± 0.10, t = 6.2, p = 0.0035, t test) and P30 (Figure 3E; contralateral = 0.67 ± 0.07, t = 9.2, p = 0.0003; ipsilateral = 0.59 ± 0.07, t = 8.8, p = 0.0003, t test) responses showed a significant bias for horizontal orientations. The horizontal orientation bias increased significantly over age for contralateral ($F_{2,13}$ = 4.8, p = 0.0269, ANOVA) and ipsilateral ($F_{2,13}$ = 30.6, p < 0.0001, ANOVA) responses. To see if this change in the neuropil is experience dependent, we measured orientation bias in the neuropil of NR and DR mice. P30 NR mice show a significant horizontal orientation bias for both contralateral and ipsilateral neuropil responses (Figure 3F; contralateral = 0.53 ± 0.09, t = 6.1, p = 0.0009; ipsilateral = 0.45 ± 0.09, t = 5.1, p = 0.0022, t test). In contrast, DR mice show no horizontal bias (Figure 3F; contralateral = −0.12 ± 0.18, t = −0.7, p = 0.5563; ipsilateral = −0.19 ± 0.27, t = −0.7, p = 0.5333, t test) and were significantly different than NR mice (contralateral, $F_{1,9}$ = 13.7, p = 0.0049; ipsilateral, F = 7.9, p = 0.0202, ANOVA). These results show that axons and dendrites within local patches of binocular neuropil develop correlated tuning to visual input from both eyes and orientation preference that requires experience, similar to the development of binocular neurons.

Arc Tunes the Development of Binocular Neurons

To gain molecular insight into the processes that regulate the development of binocularity, we investigated the role of the activity-dependent gene *Arc*. Because Arc is required for OD plasticity in V1 (Gao et al., 2010; McCurry et al., 2010), we hypothesized that Arc KO mice would mimic aspects of DR mice. We measured visual responses in binocular V1 of Arc KO mice at P14, P20, and P30 (Figure 4A; KO P14 = 34 ± 6 neurons/mouse, n = 6; P20 = 47 ± 14 neurons/mouse, n = 3; P30 = 59 ± 8 neurons/mouse, n = 4). Because this Arc KO line has destabilized GFP knocked into the endogenous Arc locus (Wang et al., 2006), we examined the fluorescence during gray screen presentations to determine if the GFP signal would lead to a higher baseline fluorescence (see STAR Methods), possibly biasing the analysis of changes in fluorescence. However, the baseline fluorescence in Arc KO mice did not significantly differ from the WT P14, P20, and P30 data (Figure S3A; P14 WT = 214 ± 30, KO = 203 ± 17, p = 0.7603; P20 WT = 315 ± 62, KO = 244 ± 3, p = 0.3203; P30 WT = 278 ± 33, KO = 231 ± 6, p = 0.2432; t test). In KO mice, the percent of visually responsive neurons responsive solely to the contralateral eye decreased significantly over development from 85.9% ± 1.2% at P14 to 41.5% ± 3.2% at P30 (Figure 4B; P20 = 70.9% ± 4.2%, $F_{2,10}$ = 88.3, p < 0.0001, ANOVA), whereas binocular responsive neurons increased significantly from 2.0% ± 1.0% at P14 to 29.2% ± 3.9% at P30 (Figure 4B; P20 = 11.5% ± 4.4%, $F_{2,10}$ = 27.3, p < 0.0001, ANOVA). Monocular ipsilateral responsive neurons also increased significantly from 12.0% ± 1.9% at P14 to 29.3% ± 2.3% at P30 (Figure 4B; P20 = 17.6% ± 1.5%, $F_{2,10}$ = 19.5, p = 0.0004, ANOVA). The population ODI increased significantly from P14 to P20, and from P20 to P30 (Figure 4C; P14 = 0.13 ± 0.02, P20 = 0.22 ± 0.02, P30 = 0.41 ± 0.02, $F_{2,10}$ = 61.5, p < 0.0001, ANOVA). ODI of binocular neurons in Arc KO mice did not significantly change over development (Figure 4D; P14 = 0.33 ± 0.07, P20 = 0.38 ± 0.03, P30 = 0.41 ± 0.02, $F_{2,7}$ = 0.8, p = 0.4719, ANOVA). Unlike WT mice, binocular offset in Arc KO mice was high in P14 animals and decreased over the course of development (Figure S3B; P14 = 52.7 ± 2.5°, P20 = 22.6 ± 4.7°, P30 = 16.9 ± 3.2°, $F_{2,7}$ = 28.2, p = 0.0004, ANOVA).

When directly compared, there is no significant difference in the percentage of visually responsive neurons between KO and WT littermates at P30 (Figure S3C; WT = 39.6% ± 0.9%, KO = 41.1% ± 2.8%, $F_{1,8}$ = 0.3, p = 0.5825, ANOVA). However, the percentage of visually responsive neurons that are binocular is significantly higher in Arc KO mice than in WT at P30 (Figure 4E; WT = 16.6% ± 2.1%, KO = 29.2% ± 3.9%, $F_{1,8}$ = 9.8, p = 0.0141, ANOVA). Additionally, the percentage of visually responsive neurons responding solely to the contralateral eye was significantly lower in Arc KO mice than in WT mice (Figure 4E; WT = 60.0% ± 3.5%, KO = 41.5% ± 3.2%, $F_{1,8}$ = 13.7, p = 0.0060, ANOVA). The ODI of the neuronal population was significantly higher in Arc KO mice than in WT (Figure 4F; WT = 0.30 ± 0.02, KO = 0.41 ± 0.02, $F_{1,8}$ = 11.6, p = 0.0093, ANOVA), whereas ODI specifically in binocular neurons did not significantly differ (Figure 4G; WT = 0.38 ± 0.03, KO = 0.41 ± 0.02, $F_{1,8}$ = 0.3, p = 0.6174, ANOVA). We next compared the visual response properties of binocular neurons in P30 WT and Arc KO mice. We found no significant differences between geneotypes (Figures 4H–4J). Finally, binocular offset did not differ between P30 WT and Arc KO mice (Figure S3D; WT = 23.6 ± 2.4°, KO = 16.9 ± 3.2°, $F_{1,8}$ = 2.8, p = 0.1333, ANOVA).

In contrast to our original hypothesis, these results show that Arc KO mice do not mirror the effect of DR. The loss of Arc results in an increase in binocular and a decrease in contralateral monocular neurons without impacting other response properties. These findings suggest that Arc may normally tune cortical circuits during development by mediating eye-specific synaptic plasticity.

Arc Tunes Binocular Neurons in the Adult Binocular Visual Cortex

Arc protein expression in V1 peaks during the critical period (Jenks et al., 2017), and we predicted that Arc's role in regulating binocular neurons would be constrained to early development. However, OD plasticity still occurs in the adult mouse visual cortex (Sawtell et al., 2003), suggesting the balance of input between the two eyes is still plastic and may require ongoing maintenance. To determine whether the maintenance of binocular cells in adult binocular V1 requires Arc, we used a floxed Arc line (Arc conditional knockout [cKO]) mice (Chen et al., 2018) crossed into the thy1-GCaMP6s line. At P180, we injected either Adeno-associated virus serotype 5 (AAV5)-hSyn-mCherry (control) or AAV5-hSyn-mCherry-Cre (AAV-Cre) virus into L2/3 of binocular V1. Immunohistochemistry of the injected hemisphere confirmed the loss of Arc protein in AAV-Cre-expressing cells (Figure S4A). As in P30 mice, a mix of monocular and binocular neurons was visible in L2/3 of AAV-Cre-injected mice (Figure 5A). The total percentage of responsive neurons did not differ between control and AAV-Cre mice (Figure S4B; Control = 55 ± 7 neurons/mouse, 37.2% ± 2.9%, n = 5; AAV-Cre = 56 ± 6 neurons/mouse, 33.5% ± 3.5%, n = 5; $F_{1,8}$ = 0.7, p = 0.4403,

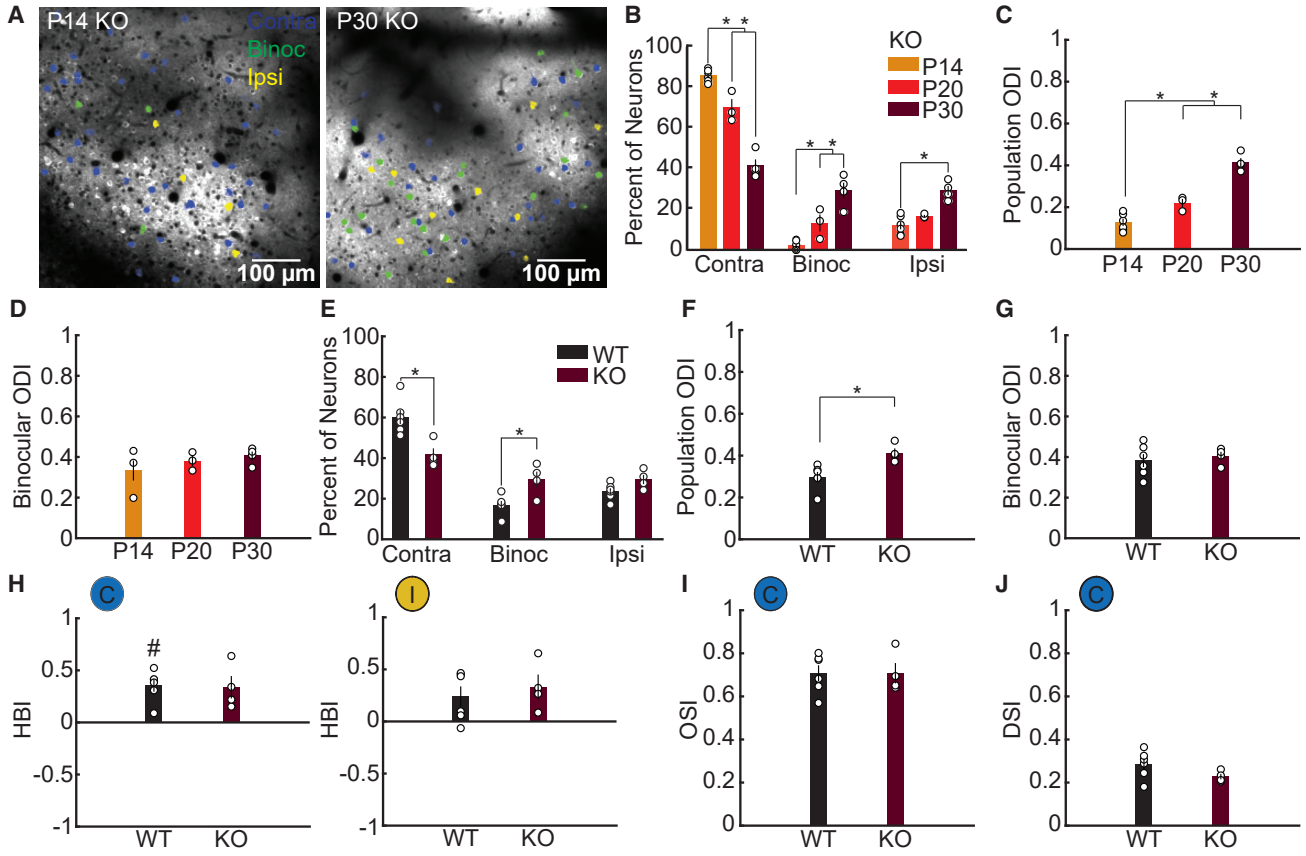

Figure 4. Arc Limits the Emergence of Binocular Neurons Early in Development

(A) Representative images from two-photon recording of visually evoked calcium responses in Arc KO mice.

(B) Percentage of visually responsive neurons that are monocular or binocular in Arc KO mice across age.

(C) ODI of the total visually responsive neuron population in Arc KO mice.

(D) ODI of binocular neurons in Arc KO mice.

(E) Percentage of visually responsive neurons that are monocular or binocular in P30 WT and Arc KO mice.

(F) ODI of the neuronal population in P30 WT and Arc KO mice.

(G) ODI in binocular neurons of P30 WT and Arc KO mice.

(H) HBI of responses in binocular neurons of P30 WT and Arc KO mice.

(I) OSI of contralateral responses in binocular neurons of P30 WT and Arc KO mice.

(J) DSI of contralateral responses in binocular neurons of P30 WT and Arc KO mice (*$p < 0.05$ indicates a significant difference between groups; #$p < 0.05$ indicates a significant difference within a group from the expected mean; error bars represent standard error of the mean; open circles indicate a data point from an individual mouse; n = number of animals for all statistics).

See also Figure S3.

ANOVA). Strikingly, AAV-Cre-mediated knockdown of Arc in adult binocular V1 was sufficient to alter the percentage of binocular neurons compared to control-injected mice (Figure 5B; control = 12.6 ± 2.5%; AAV-Cre = 26.6 ± 5.3%; $F_{1,8}$ = 5.7, p = 0.0442, ANOVA). Additionally, AAV-Cre-injected mice showed a decrease in the number of monocular contralateral neurons (Figure 5B; control = 70.7 ± 4.8%; AAV-Cre = 40.6 ± 6.2%; $F_{1,8}$ = 14.7, p = 0.0050, ANOVA) and an increase in monocular ipsilateral neurons (Figure 5B; control = 16.6 ± 4.1%; AAV-Cre = 32.8 ± 3.6%; $F_{1,8}$ = 8.8, p = 0.0180, ANOVA). Consistent with an overall shift in binocularity, AAV-Cre-injected mice also showed an increase in the ODI of the neuronal population (Figure 5C; control = 0.24 ± 0.06; AAV-Cre = 0.43 ± 0.05; $F_{1,8}$ = 6.4, p = 0.0356, ANOVA). The ODI of binocular neurons was unaffected (Figure 5D; control = 0.41 ± 0.02; AAV-Cre = 0.35 ± 0.03; $F_{1,8}$ = 2.6, p = 0.1442, ANOVA). We next compared the response properties of binocular neurons in control- and AAV-Cre-injected mice. As expected, binocular neurons in control-injected mice showed an orientation preference bias for horizontal orientations (Figure 5E; contralateral = 0.39 ± 0.12, t = 3.2, p = 0.0331; ipsilateral = 0.44 ± 0.09, t = 4.7, p = 0.0096; t test). Although this bias was still present in contralateral responses of AAV-Cre mice (AAV-Cre = 0.18 ± 0.05, t = 3.4, p = 0.0261, t test; comparison to control, $F_{1,8}$ = 2.5, p = 0.1514, ANOVA), it was absent in ipsilateral responses (AAV-Cre = 0.09 ± 0.04, t = 2.0, p = 0.1209, t test) and significantly differed from control

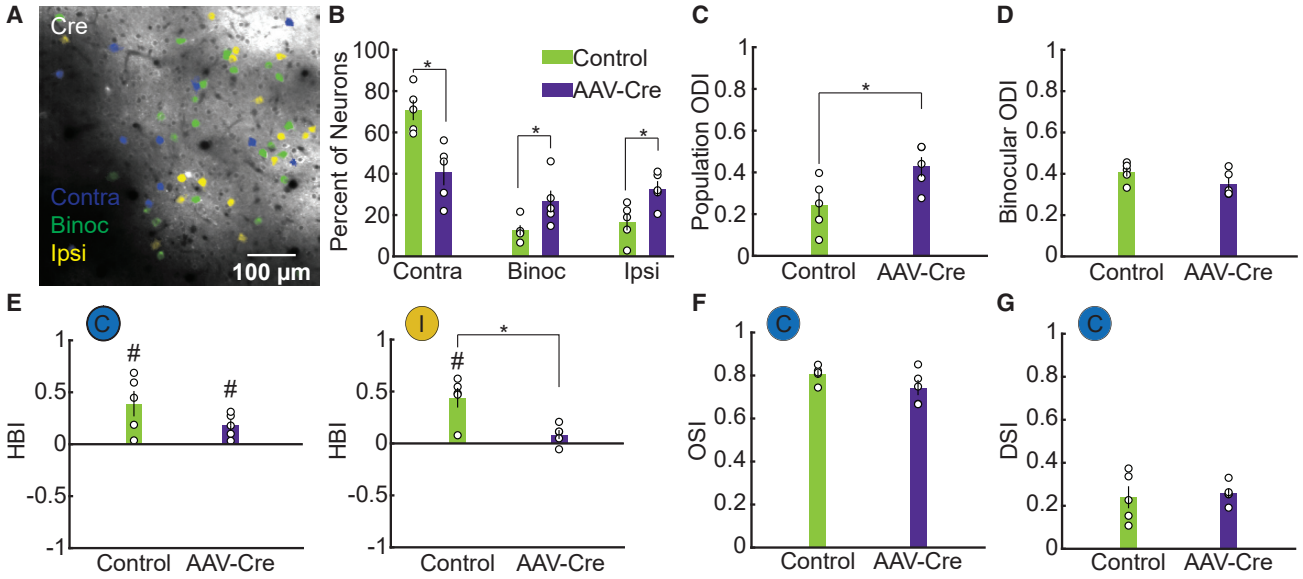

Figure 5. Arc Is Required for the Maintenance of Binocular Neuron Number in Adult Binocular V1

(A) Representative image from a two-photon recording of visually evoked calcium responses from neurons in an AAV-Cre-injected mouse.

(B) Percentage of visually responsive neurons that are monocular or binocular in control and AAV-Cre mice.

(C) ODI of the total population of neurons in control and AAV-Cre mice.

(D) ODI of binocular neurons in control and AAV-Cre mice.

(E) HBI of responses in binocular neurons.

(F) OSI of contralateral responses in binocular neurons.

(G) DSI of contralateral responses in binocular neurons (*$p < 0.05$ indicates a significant difference between groups; #$p < 0.05$ indicates a significant difference within a group from the expected mean; error bars represent standard error of the mean; open circles indicate a data point from an individual mouse; n = number of animals for all statistics).

See also Figure S4.

mice ($F_{1,8} = 11.6$, $p = 0.0092$, ANOVA). Neither contralateral OSI (Figure 5F; control = 0.81 ± 0.02; AAV-Cre = 0.74 ± 0.04; $F_{1,8} = 2.6$, $p = 0.1466$, ANOVA) or contralateral DSI (Figure 5G; control = 0.24 ± 0.05; AAV-Cre = 0.26 ± 0.02; $F_{1,8} = 0.1$, $p = 0.7430$, ANOVA) differed between control and AAV-Cre mice. Binocular offset was also not significantly different between control- and AAV-Cre-injected mice (Figure S4C; control = 19.7 ± 0.9°; AAV-Cre = 25.9 ± 2.7°; $F_{1,8} = 4.6$, $p = 0.0642$, ANOVA). See Table S1 for a summary of all response properties across genotype and manipulation.

These results show that acutely reducing Arc levels in adult binocular V1, surprisingly, recapitulates the developmental phenotype observed in full Arc KO mice. Thus, Arc controls the percentage of binocular neurons even in adult V1. This suggests that the precise regulation of binocularity requires ongoing maintenance and plasticity in adult V1.

DISCUSSION

The interplay between experience and genetic hardwiring of circuits in the brain results in the optimal processing of information from the outside world. Here, we show that at eye-opening the mouse binocular V1 is mostly driven by monocular responding cells, and binocular cells rapidly emerge after eye-opening in an experience-dependent process that is, in part, regulated by the activity-dependent gene *Arc*. These binocular neurons convey specific visual response properties, including a bias for horizontal orientations. The emergence of binocular responding neurons is associated with an increase in total correlated activity between the two eyes in the neuropil, which is also experience dependent. These data solidify the role of experience in early development as a crucial component of refining sensory processing required for binocular vision.

Although it is clear that there are critical windows of plasticity during development that are essential for normal wiring of neuronal circuits, it has also become evident that brain plasticity still occurs in adult brains (Hübener and Bonhoeffer, 2014). Indeed, many studies have reinstated juvenile-like plasticity in adult brains through manipulations of experience, genetics, or pharmacology (Greifzu et al., 2014; He et al., 2006; Jenks et al., 2017; Matthies et al., 2013; Pizzorusso et al., 2002; Maya Vetencourt et al., 2008). However, few studies have shown a direct role for plasticity in regulating or maintaining circuits required for sensory processing in adults. Unexpectedly, we found that acute knockdown of Arc in adult mouse binocular V1 alters the distribution of monocular and binocular neurons, recapitulating the developmental phenotype of an increased percentage of binocular neurons observed in young Arc KO mice. These results suggest that sensory circuits may require

ongoing plasticity that refines information processing in response to experience, even in adult brains.

Binocularity Develops after Eye-Opening

Previous studies that have evaluated binocular V1 in mice have predominately used methods that lack single-cell resolution (intrinsic or wide-field imaging and local field potentials) or have issues with sampling bias (single unit electrophysiology). We found, at the single-cell level, that at eye-opening L2/3 neurons in binocular V1 are mostly monocular responding cells (~90%) and that by P30 there are ~80% monocular/~20% binocular cells, which remains constant into adulthood. This high prevalence of monocular cells in binocular V1 is similar to what has been previously observed using GCaMP6 recordings (Jaepel et al., 2017; Salinas et al., 2017). However, it is possible that because the transgenic Thy1-GCaMP6 expression is lower than the viral expression of GCaMP6 we may miss very weak responses that would lead to the under-estimation of binocular cell numbers (Dana et al., 2014). Additionally, there may be some bias in the population of cells expressing GCaMP, as not every L2/3 neuron expresses the transgene. However, Thy1-GCaMP6s 4.3 mice have been used in several studies to examine visual responses of excitatory neurons (Dana et al., 2014; Lee et al., 2017; Park et al., 2017; Sun et al., 2016). Sun et al. (2016) report that of 2,608 L2/3 neurons analyzed from 6 Thy1-GCaMP6 GP4.3 mice, 1,279 (49%) were visually responsive, consistent with our findings in P30 mice, and Dana et al. (2014) report that ~80% of all L2/3 neurons are labeled in V1, indicating that the labeled neurons make up the majority of excitatory neurons.

Although the percentage of binocular neurons is low, the emergence of binocular neurons coincides with an increase in the correlation between contralateral and ipsilateral input in the neuropil. Calcium signals in large (~10,000 μm^2) sections of neuropil correlate well with electrocorticogram measures of sensory-evoked population activity (Kerr et al., 2005). However, smaller sections of neuropil can report stimulus-specific information with response properties comparable to neurons in the same area (Lee et al., 2017). Although this local specificity is incompatible with the view of mouse V1 as a "salt and pepper" mix of orientation preference, this finding agrees with the observation that neurons with similar tuning lie close together and that thalamocortical projections from LGN to V1 arrange in patches rather than having no spatial organization (Ji et al., 2015; Ringach et al., 2016). Similarly tuned neurons preferentially wire together, and the probability for similarly tuned neurons to be connected doubles over development from P13–15 to P22–26 (Ko et al., 2013). Our findings demonstrate that spatial organization of orientation preference becomes "aligned" between the two eyes during development, mirroring the emergence of binocular neurons. It will be of interest to examine the contribution of neurons in and projecting to L2/3 of binocular V1 to the refinement of visual responses in the neuropil. Additionally, the prevalence of robust neuropil responses to visual stimuli highlights the importance of neuropil subtraction in isolating accurate somatic responses.

Because our recordings are acute, we were not able to follow the same neurons over time to determine if previously monocular neurons become binocular. Neurons could become binocular by the addition or strengthening of ipsilateral eye input into V1, i.e., a switch from monocular contralateral to binocular. Alternatively, neurons that start as monocularly ipsilateral could switch to binocular by the addition or strengthening of contralateral input. Surprisingly, we did not find a developmental change in binocular matching in WT mice after eye-opening. To our knowledge, the only other studies showing mismatched orientation preferences specifically in L2/3 have been following monocular deprivation (Levine et al., 2017) or after silencing of interneurons (Yaeger et al., 2019), not during normal development. The development of binocular matching may occur mostly in thalamic inputs or in L4 neurons that innervate L2/3. Thus, the binocular neurons that develop in L2/3 may already receive matched input that does not undergo further refinement. Additionally, the use of GCaMP calcium imaging rather than electrophysiological recordings may miss weaker inputs that are mismatched.

Experience Shapes the Development of Binocularity

Much of what is known about experience-dependent plasticity in V1 comes from monocular deprivation studies. Less is known about the activity-dependent processes that regulate normal development of visual response properties in binocular V1. We find that the development and tuning of binocular neurons are experience dependent in mouse V1. DR mice lack both the increase in binocular neurons and the horizontal orientation bias in binocular neurons. The increase in correlated binocular activity in the neuropil is also experience dependent. Interestingly, of the developmental changes in binocular neurons, only orientation selectivity is not experience dependent. Refinement of orientation selectivity may be due to processes that occur before eye-opening or predominantly in L4 or even thalamic input from the lateral geniculate nucleus (Jaepel et al., 2017). It is unclear how conserved these mechanisms are in other species that have binocular vision.

Experience and the induction of activity-dependent gene expression are tightly coupled. The immediate early gene Arc is necessary for experience-dependent synaptic plasticity in mouse V1 (McCurry et al., 2010), and Arc overexpression is sufficient to prolong or re-open the critical period of OD plasticity (Jenks et al., 2017). Here, we tested whether Arc regulates the normal development of visual response properties. We find that Arc expression regulates the normal distribution of monocular and binocular neurons in binocular V1. Surprisingly, Arc KO mice show a significant increase in binocular neurons compared with WT mice, which is the opposite of what occurs in DR mice. Additionally, Arc KO mice show decreased monocular neurons. Thus, at the population level, there is a change in overall OD where the contralateral and ipsilateral drive is more equivalent than the contralateral dominance observed in WT mice. Consistent with this, ODI derived from visually evoked potentials shows that Arc KO mice at the population level have a ~1:1 contralateral to ipsilateral response amplitude ratio as opposed to the ~2:1 ratio in WT mice (McCurry et al., 2010).

Arc is implicated in various forms of synaptic plasticity, such as LTP/LTD and homeostatic scaling of α-amino-3-hydroxy-5-methyl-4-isoxazolepropionic acid (AMPA) receptors (Shepherd and Bear, 2011). Arc KO mice lack OD plasticity following monocular deprivation (McCurry et al., 2010) and the scaling of

mini excitatory postsynaptic currents (mEPSCs) following dark adaptation (Gao et al., 2010). Both phenotypes suggest deficits in downscaling or weakening of non-correlated/inactive synaptic inputs. Contralateral input matures before ipsilateral input in the binocular visual cortex (Smith and Trachtenberg, 2007) and is thought to guide, but also compete with, ipsilateral input as ipsilateral maturation accelerates in the absence of contralateral input. We hypothesize that one way that contralateral input limits ipsilateral development is through homeostatic regulation of total output of the cell, leading to synaptic downscaling and suppressing the addition of new, ipsilateral inputs. Because Arc is required for downscaling, neurons that lack Arc could gain additional ipsilateral inputs during development that lead to more binocular neurons and fewer contralateral monocular neurons. An alternative model is that binocular neurons initially arise from potentiation or an increase in ipsilateral input during development that is then subsequently refined by LTD processes. Because Arc is also required for LTD in the visual cortex (Jenks et al., 2017), neurons that would have otherwise become contralateral responsive only in a WT mouse become binocular in an Arc KO mouse due to the lack of LTD of ipsilateral input.

In addition to cell-autonomous processes, Arc may also have a brain-wide role in regulating experience-dependent correlated activity in different brain regions during development (Kraft et al., 2017), which may occur through non-cell-autonomous regulation of synaptic plasticity through the intercellular spread of Arc protein capsids (Pastuzyn et al., 2018). Further studies will be required to determine precisely how Arc regulates cellular changes in V1 neurons.

Sensory Circuits in the Visual Cortex Are Maintained by Synaptic Plasticity in Adult Animals

Experience-dependent plasticity has been well documented in the adult brain, although, in general, the extent and ease of induction are limited compared with the juvenile brain (Hübener and Bonhoeffer, 2014). Therefore, the role of experience-dependent plasticity in regulating adult sensory processing is thought to be restricted. However, manipulations of experience, such as dark exposure, can reactivate developmental plasticity and allow recovery from developmental deficits, such as amblyopia (He et al., 2007), suggesting that the adult cortex is still primed to undergo experience-dependent plasticity. Here, we find that reducing Arc levels in the adult cortex and well beyond the classical critical period in mice resulted in a significant change in the distribution of monocular and binocular neurons. These changes were observed in a relatively short time course of Arc knockdown (~2 weeks) and recapitulate the developmental observation that the absence of Arc increases the percentage of visually responsive neurons that are binocular. These results show that the ongoing maintenance of binocular circuits in adult V1 requires Arc-dependent plasticity.

The increase in the percentage of binocular and ipsilateral monocular neurons in Arc KO adult V1 is intriguing and reminiscent of earlier observations that removal of the contralateral eye in P180 mice allows further refinement and strengthening of ipsilateral responses (Smith and Trachtenberg, 2010). Because contralateral monocular neurons decreased in Arc KO V1 (with no change in the overall percentage of neurons responsive), we speculate that continued Arc expression in adulthood is required for contralateral inputs to maintain dominance over the ipsilateral eye. This could occur through local, heterosynaptic competition between spines serving the contralateral and ipsilateral eye, which has been observed in paradigms such as recovery following monocular deprivation (El-Boustani et al., 2018). Arc may preferentially weaken ipsilateral input; thus, without Arc, the relative ratio of contra- to ipsilateral inputs becomes more equal. Chronic imaging of the same neurons before and after Arc deletion may help resolve precisely how binocularity is maintained.

Our findings show that experience is required for the emergence and tuning of V1 binocular neurons during development and that similar experience-dependent plasticity is required for the ongoing maintenance of binocularity in adult V1.

STAR★METHODS

Detailed methods are provided in the online version of this paper and include the following:

- KEY RESOURCES TABLE
- LEAD CONTACT AND MATERIALS AVAILABILITY
- EXPERIMENTAL MODEL AND SUBJECT DETAILS
  - Mouse models
- METHOD DETAILS
  - Cranial window Surgeries
  - Virus injections
  - Immunohistochemistry
  - Retinotopic mapping
  - Two-photon calcium imaging
- QUANTIFICATION AND STATISTICAL ANALYSIS
  - Analysis of retinotopy data
  - Analysis of two-photon imaging data
- DATA AND CODE AVAILABILITY

SUPPLEMENTAL INFORMATION

Supplemental Information can be found online at https://doi.org/10.1016/j.celrep.2020.01.031.

ACKNOWLEDGMENTS

We thank Dr. Richard Palmiter (University of Washington) for the gift of the Arc conditional KO mouse line and Dr. Kuan Wang (National Institutes of Health [NIH]) for the Arc KO line. We thank the Wachowiak lab for helpful discussions and technical help with two-photon imaging. K.R.J. was supported by the University of Utah Neuroscience Training Program (5T32NS076067) and by the NIH (F31-MH112326). This work was funded by the NIH (to J.D.S.; R00-NS076364 and R01-MH112766) and the E. Matilda Ziegler Foundation (J.D.S.).

AUTHOR CONTRIBUTIONS

Conceptualization, K.R.J. and J.D.S.; Methodology, K.R.J. and J.D.S.; Software, K.R.J.; Investigation, K.R.J.; Writing, K.R.J. and J.D.S.; Funding Acquisition, K.R.J. and J.D.S.; Supervision, J.D.S.

DECLARATION OF INTERESTS

The authors declare no competing interests.

Received: April 24, 2019
Revised: November 25, 2019
Accepted: January 8, 2020
Published: February 11, 2020

REFERENCES

Chen, J.Y., Campos, C.A., Jarvie, B.C., and Palmiter, R.D. (2018). Parabrachial CGRP Neurons Establish and Sustain Aversive Taste Memories. Neuron *100*, 891–899.e5.

Crair, M.C., Gillespie, D.C., and Stryker, M.P. (1998). The role of visual experience in the development of columns in cat visual cortex. Science *279*, 566–570.

Dana, H., Chen, T.W., Hu, A., Shields, B.C., Guo, C., Looger, L.L., Kim, D.S., and Svoboda, K. (2014). Thy1-GCaMP6 transgenic mice for neuronal population imaging *in vivo*. PLoS One *9*, e108697.

Dräger, U.C. (1975). Receptive fields of single cells and topography in mouse visual cortex. J. Comp. Neurol. *160*, 269–290.

El-Boustani, S., Ip, J.P.K., Breton-Provencher, V., Knott, G.W., Okuno, H., Bito, H., and Sur, M. (2018). Locally coordinated synaptic plasticity of visual cortex neurons in vivo. Science *360*, 1349–1354.

Espinosa, J.S., and Stryker, M.P. (2012). Development and plasticity of the primary visual cortex. Neuron *75*, 230–249.

Feng, G., Mellor, R.H., Bernstein, M., Keller-Peck, C., Nguyen, Q.T., Wallace, M., Nerbonne, J.M., Lichtman, J.W., and Sanes, J.R. (2000). Imaging neuronal subsets in transgenic mice expressing multiple spectral variants of GFP. Neuron *28*, 41–51.

Figueroa Velez, D.X., Ellefsen, K.L., Hathaway, E.R., Carathedathu, M.C., and Gandhi, S.P. (2017). Contribution of innate cortical mechanisms to the maturation of orientation selectivity in Parvalbumin interneurons. J. Neurosci. *37*, 820–829.

Gao, M., Sossa, K., Song, L., Errington, L., Cummings, L., Hwang, H., Kuhl, D., Worley, P., and Lee, H.K. (2010). A specific requirement of Arc/Arg3.1 for visual experience-induced homeostatic synaptic plasticity in mouse primary visual cortex. J. Neurosci. *30*, 7168–7178.

Greifzu, F., Pielecka-Fortuna, J., Kalogeraki, E., Krempler, K., Favaro, P.D., Schlüter, O.M., and Löwel, S. (2014). Environmental enrichment extends ocular dominance plasticity into adulthood and protects from stroke-induced impairments of plasticity. Proc. Natl. Acad. Sci. USA *111*, 1150–1155.

Gu, Y., Huang, S., Chang, M.C., Worley, P., Kirkwood, A., and Quinlan, E.M. (2013). Obligatory role for the immediate early gene NARP in critical period plasticity. Neuron *79*, 335–346.

Hagihara, K.M., Murakami, T., Yoshida, T., Tagawa, Y., and Ohki, K. (2015). Neuronal activity is not required for the initial formation and maturation of visual selectivity. Nat. Neurosci. *18*, 1780–1788.

He, H.Y., Hodos, W., and Quinlan, E.M. (2006). Visual deprivation reactivates rapid ocular dominance plasticity in adult visual cortex. J. Neurosci. *26*, 2951–2955.

He, H.Y., Ray, B., Dennis, K., and Quinlan, E.M. (2007). Experience-dependent recovery of vision following chronic deprivation amblyopia. Nat. Neurosci. *10*, 1134–1136.

Hoy, J.L., and Niell, C.M. (2015). Layer-specific refinement of visual cortex function after eye opening in the awake mouse. J. Neurosci. *35*, 3370–3383.

Hubel, D.H., Wiesel, T.N., and LeVay, S. (1976). Functional architecture of area 17 in normal and monocularly deprived macaque monkeys. Cold Spring Harb. Symp. Quant. Biol. *40*, 581–589.

Hübener, M., and Bonhoeffer, T. (2014). Neuronal plasticity: beyond the critical period. Cell *159*, 727–737.

Jaepel, J., Hübener, M., Bonhoeffer, T., and Rose, T. (2017). Lateral geniculate neurons projecting to primary visual cortex show ocular dominance plasticity in adult mice. Nat. Neurosci. *20*, 1708–1714.

Jenks, K.R., Kim, T., Pastuzyn, E.D., Okuno, H., Taibi, A.V., Bito, H., Bear, M.F., and Shepherd, J.D. (2017). Arc restores juvenile plasticity in adult mouse visual cortex. Proc. Natl. Acad. Sci. USA *114*, 9182–9187.

Jeon, B.B., Swain, A.D., Good, J.T., Chase, S.M., and Kuhlman, S.J. (2018). Feature selectivity is stable in primary visual cortex across a range of spatial frequencies. Sci. Rep. *8*, 15288.

Ji, W., Gămănuț, R., Bista, P., D'Souza, R.D., Wang, Q., and Burkhalter, A. (2015). Modularity in the Organization of Mouse Primary Visual Cortex. Neuron *87*, 632–643.

Kalatsky, V.A., and Stryker, M.P. (2003). New paradigm for optical imaging: temporally encoded maps of intrinsic signal. Neuron *38*, 529–545.

Keck, T., Keller, G.B., Jacobsen, R.I., Eysel, U.T., Bonhoeffer, T., and Hübener, M. (2013). Synaptic scaling and homeostatic plasticity in the mouse visual cortex *in vivo*. Neuron *80*, 327–334.

Kerr, J.N.D., Greenberg, D., and Helmchen, F. (2005). Imaging input and output of neocortical networks in vivo. Proc. Natl. Acad. Sci. USA *102*, 14063–14068.

Ko, H., Cossell, L., Baragli, C., Antolik, J., Clopath, C., Hofer, S.B., and Mrsic-Flogel, T.D. (2013). The emergence of functional microcircuits in visual cortex. Nature *496*, 96–100.

Kraft, A.W., Mitra, A., Bauer, A.Q., Snyder, A.Z., Raichle, M.E., Culver, J.P., and Lee, J.-M. (2017). Visual experience sculpts whole-cortex spontaneous infraslow activity patterns through an Arc-dependent mechanism. Proc. Natl. Acad. Sci. USA *114*, E9952–E9961.

Lee, S., Meyer, J.F., Park, J., and Smirnakis, S.M. (2017). Visually Driven Neuropil Activity and Information Encoding in Mouse Primary Visual Cortex. Front. Neural Circuits *11*, 50.

Levelt, C.N., and Hübener, M. (2012). Critical-period plasticity in the visual cortex. Annu. Rev. Neurosci. *35*, 309–330.

Levine, J.N., Chen, H., Gu, Y., and Cang, J. (2017). Environmental Enrichment Rescues Binocular Matching of Orientation Preference in the Mouse Visual Cortex. J. Neurosci. *37*, 5822–5833.

Li, Y., Fitzpatrick, D., and White, L.E. (2006). The development of direction selectivity in ferret visual cortex requires early visual experience. Nat. Neurosci. *9*, 676–681.

Matthies, U., Balog, J., and Lehmann, K. (2013). Temporally coherent visual stimuli boost ocular dominance plasticity. J. Neurosci. *33*, 11774–11778.

Maya Vetencourt, J.F., Sale, A., Viegi, A., Baroncelli, L., De Pasquale, R., O'Leary, O.F., Castrén, E., and Maffei, L. (2008). The antidepressant fluoxetine restores plasticity in the adult visual cortex. Science *320*, 385–388.

McCurry, C.L., Shepherd, J.D., Tropea, D., Wang, K.H., Bear, M.F., and Sur, M. (2010). Loss of Arc renders the visual cortex impervious to the effects of sensory experience or deprivation. Nat. Neurosci. *13*, 450–457.

Murakami, T., Matsui, T., and Ohki, K. (2017). Functional Segregation and Development of Mouse Higher Visual Areas. J. Neurosci. *37*, 9424–9437.

Niell, C.M., and Stryker, M.P. (2008). Highly selective receptive fields in mouse visual cortex. J. Neurosci. *28*, 7520–7536.

Park, J.H., Kong, L., Zhou, Y., and Cui, M. (2017). Large-field-of-view imaging by multi-pupil adaptive optics. Nat. Methods *14*, 581–583.

Pastuzyn, E.D., Day, C.E., Kearns, R.B., Kyrke-Smith, M., Taibi, A.V., McCormick, J., Yoder, N., Belnap, D.M., Erlendsson, S., Morado, D.R., et al. (2018). The Neuronal Gene Arc Encodes a Repurposed Retrotransposon Gag Protein that Mediates Intercellular RNA Transfer. Cell *172*, 275–288.e18.

Peron, S.P., Freeman, J., Iyer, V., Guo, C., and Svoboda, K. (2015). A Cellular Resolution Map of Barrel Cortex Activity during Tactile Behavior. Neuron *86*, 783–799.

Pizzorusso, T., Medini, P., Berardi, N., Chierzi, S., Fawcett, J.W., and Maffei, L. (2002). Reactivation of ocular dominance plasticity in the adult visual cortex. Science *298*, 1248–1251.

Rakic, P. (1976). Prenatal genesis of connections subserving ocular dominance in the rhesus monkey. Nature *261*, 467–471.

Ramesh, R.N., Burgess, C.R., Sugden, A.U., Gyetvan, M., and Andermann, M.L. (2018). Intermingled Ensembles in Visual Association Cortex Encode Stimulus Identity or Predicted Outcome. Neuron *100*, 900–915.e9.

Ringach, D.L., Mineault, P.J., Tring, E., Olivas, N.D., Garcia-Junco-Clemente, P., and Trachtenberg, J.T. (2016). Spatial clustering of tuning in mouse primary visual cortex. Nat. Commun. *7*, 12270.

Rochefort, N.L., Narushima, M., Grienberger, C., Marandi, N., Hill, D.N., and Konnerth, A. (2011). Development of direction selectivity in mouse cortical neurons. Neuron *71*, 425–432.

Salinas, K.J., Figueroa Velez, D.X., Zeitoun, J.H., Kim, H., and Gandhi, S.P. (2017). Contralateral bias of high spatial frequency tuning and cardinal direction selectivity in mouse visual cortex. J. Neurosci. *37*, 10125–10138.

Sawtell, N.B., Frenkel, M.Y., Philpot, B.D., Nakazawa, K., Tonegawa, S., and Bear, M.F. (2003). NMDA receptor-dependent ocular dominance plasticity in adult visual cortex. Neuron *38*, 977–985.

Scholl, B., Pattadkal, J.J., and Priebe, N.J. (2017). Binocular Disparity Selectivity Weakened after Monocular Deprivation in Mouse V1. J. Neurosci. *37*, 6517–6526.

Shepherd, J.D., and Bear, M.F. (2011). New views of Arc, a master regulator of synaptic plasticity. Nat. Neurosci. *14*, 279–284.

Sherk, H., and Stryker, M.P. (1976). Quantitative study of cortical orientation selectivity in visually inexperienced kitten. J. Neurophysiol. *39*, 63–70.

Smith, S.L., and Trachtenberg, J.T. (2007). Experience-dependent binocular competition in the visual cortex begins at eye opening. Nat. Neurosci. *10*, 370–375.

Smith, S., and Trachtenberg, J. (2010). The refinement of ipsilateral eye retinotopic maps is increased by removing the dominant contralateral eye in adult mice. PLoS ONE *5*, e9925.

Stringer, C., Pachitariu, M., Steinmetz, N., Reddy, C.B., Carandini, M., and Harris, K.D. (2019). Spontaneous behaviors drive multidimensional, brainwide activity. Science *364*, 255.

Sun, W., Tan, Z., Mensh, B.D., and Ji, N. (2016). Thalamus provides layer 4 of primary visual cortex with orientation- and direction-tuned inputs. Nat. Neurosci. *19*, 308–315.

Tagawa, Y., Kanold, P.O., Majdan, M., and Shatz, C.J. (2005). Multiple periods of functional ocular dominance plasticity in mouse visual cortex. Nat. Neurosci. *8*, 380–388.

Wang, K.H., Majewska, A., Schummers, J., Farley, B., Hu, C., Sur, M., and Tonegawa, S. (2006). *In vivo* two-photon imaging reveals a role of arc in enhancing orientation specificity in visual cortex. Cell *126*, 389–402.

Wang, B.S., Sarnaik, R., and Cang, J. (2010). Critical period plasticity matches binocular orientation preference in the visual cortex. Neuron *65*, 246–256.

Wang, B.S., Feng, L., Liu, M., Liu, X., and Cang, J. (2013). Environmental enrichment rescues binocular matching of orientation preference in mice that have a precocious critical period. Neuron *80*, 198–209.

Yaeger, C.E., Ringach, D.L., and Trachtenberg, J.T. (2019). Neuromodulatory control of localized dendritic spiking in critical period cortex. Nature *567*, 100–104.

Yoon, B.-J., Smith, G.B., Heynen, A.J., Neve, R.L., and Bear, M.F. (2009). Essential role for a long-term depression mechanism in ocular dominance plasticity. Proc. Natl. Acad. Sci. USA *106*, 9860–9865.

Zhuang, J., Ng, L., Williams, D., Valley, M., Li, Y., Garrett, M., and Waters, J. (2017). An extended retinotopic map of mouse cortex. eLife *6*, 1–29.

STAR★METHODS

KEY RESOURCES TABLE

REAGENT or RESOURCE	SOURCE	IDENTIFIER
Antibodies		
Arc/Arg3.1 rabbit polyclonal	Proteintech	Cat#16290-1-AP; RRID: AB_2151832
Alexa Fluor donkey anti-rabbit 488	Jackson ImmunoResearch	Cat#711-545-152; RRID: AB_2313584
Bacterial and Virus Strains		
AAV5-hSyn-mCherry	University of North Carolina Vector Core	N/A
AAV5-hSyn-mCherry-Cre	University of North Carolina Vector Core	N/A
Experimental Models: Organisms/Strains		
Mouse: Arc KO: C57BL/6-Arctm1Stl/J	Dr. Kuan Hong Wang, NIH	Jackson Laboratory Cat#007662; RRID: IMSR_JAX:007662
Mouse: Thy1 GCaMP6s: C57BL/6J-Tg(Thy1-GCaMP6s)GP4.3Dkim/J	Jackson Laboratory	Jackson Laboratory Cat#024275
Mouse: Arc cKO: B6.Cg-*Arc*$^{tm1.1Rpa}$/J	Dr. Richard Palmiter, University of Washington	Jackson Laboratory Cat#033170
Software and Algorithms		
Prairie View	Bruker	https://www.bruker.com/
Custom analysis code	This paper	https://github.com/Shepherdlab/2Photon
ImageJ	NIH	https://imagej.nih.gov/ij/
MATLAB(R2018a)	MathWorks	https://www.mathworks.com/
Suite2P(December 2018)	Howard Hughes Medical Institute Janelia Research Campus	https://mouseland.github.io/suite2p

LEAD CONTACT AND MATERIALS AVAILABILITY

Further information and requests for resources and reagents should be directed to and will be fulfilled by the Lead Contact, Jason D. Shepherd (jason.shepherd@neuro.utah.edu). This study did not generate new unique reagents.

EXPERIMENTAL MODEL AND SUBJECT DETAILS

Mouse models

Thy1-GCaMP6s mice (C57BL/6J-Tg(Thy1-GCaMP6s)GP4.3Dkim/J) were used for retinotopy, spatial frequency, and dark rearing experiments. Thy1 GCaMP6s mice were crossed into the Arc KO (GFP knocked in to the *Arc* open reading frame, C57BL/6-Arc^{tm1stl}/J, a kind gift from Dr. Kuan Wang, NIH) or Arc cKO (Cg-Arc$^{tm1.1Rpa}$/J, a kind gift from Dr. Richard Palmiter, University of Washington) mouse lines in all other experiments. All lines were backcrossed to C57BL/6J mice. Heterozygotes from the Arc KO mouse line were crossed to each other, with one parent positive for Thy1-GCaMP6s, to yield littermate WT and Arc KO mice. Arc cKO mice were bred with the Thy1-GCaMP6s mice to produce a line of Arc cKO mice positive for GCaMP6s for conditional deletion experiments at P180. Both male and female mice were used in all experiments. Mice were group-housed until the day of recording. P14 and P20 mice were kept with their dams until the day of recording. All P30 and older mice were weaned at P21. All mice, with the exception of dark reared mice, were kept on a 12h:12h light/dark cycle. Dark reared mice were housed in a separate room in a dark cabinet and checked daily using a red LED light. All mice were provided *ad libitum* food and water. All procedures were performed in compliance with and approved by the Institutional Animal Care and Use Committee at the University of Utah. All mice were checked daily by trained veterinarians and veterinary staff at the University of Utah.

METHOD DETAILS

Cranial window Surgeries

Cranial window surgeries were performed identically for all ages and genotypes used in the study. Where appropriate, the experimenter was blind to genotype. On the day of recording, mice were anesthetized with 2% isoflurane and injected subcutaneously

with enrofloxacin (7mg/kg, VETONE), Carprofren (5mg/kg, Zoetis), and Dexamethasone (0.2 mg/kg, VETONE). The fur over the scalp was trimmed, and mice secured in a stereotax (Kopf). 0.1 mL 2% lidocaine (VETONE) was injected subcutaneously under the scalp and the scalp sterilized with alternating swabs of iodine and 70% ethanol. The scalp was removed using scissors, and the skull scraped clean using a scalpel and then dried. A 3 mm circle was drawn lightly with a drill tip over the right binocular visual cortex, centered 3 mm lateral of midline and 1 mm anterior lambda. The skull outside the 3 mm circle and skin margins were covered by a layer of Vetbond (3M) and then dental cement (Lang) mixed with black acrylic paint powder (Sargent Art) and allowed to dry. A 3 mm craniotomy was carefully drilled using a high-speed drill and 0.5 mm drill bit. Ice cold ACSF (124 mM NaCl, 3.2 mM KCl, 1.25 mM NaH_2PO_4, 2 mM CaCl) was periodically placed on the site of drilling to cool the brain and clean the skull surface. When only a thin layer of bone remained at the margins of the craniotomy, forceps were used to remove the circle of bone under a drop of ACSF. ACSF was used to wash the brain surface until surface bleeding was controlled. In some cases, Gelfoam (Pzfizer) was placed on the brain surface to remove excess blood. When bleeding had stopped, a 3 mm circular coverslip (No. 0 coverglass, Warner Instruments) was placed on the brain surface and held down using a needle attached to the arm of the stereotax. Vetbond and dental cement were used to attach the edges of the coverglass to the skull. A custom stainless steel headplate was attached to the skull using dental cement. Animals were allowed to recover on a heating pad and given a post-surgery injection of carprofen subcutaneously to control pain. All animals were allowed to recover for at least 3 h prior to imaging. For dark rearing experiments, both dark reared animals and normally reared controls recovered in a dark cabinet, and transportation was carried out in the dark with no light exposure until the animal was under anesthesia.

Virus injections

For Arc conditional knock out studies, either AAV5-hSyn-mCherry or AAV5-hSyn-mCherry-Cre were injected into V1 of Thy1 GCaMP6s Arc cKO mice at concentrations of 10^{12} GC/mL (University of North Carolina Viral Vector Core). Mice were anesthetized with 2% isoflurane (VETONE) and injected subcutaneously with enrofloxacin (7mg/kg, VETONE), Carprofren (5mg/kg, Zoetis) and Dexamethasone (0.2 mg/kg, VETONE). The fur over the scalp was trimmed, and mice secured in a stereotax (Kopf). 0.1 mL 2% lidocaine (VETONE) was injected subcutaneously under the scalp and the scalp sterilized with alternating swabs of iodine and 70% ethanol. A small incision was then made to expose the skull surface and the position of the right, binocular visual cortex marked (3 mm lateral midline, 1 mm anterior Lambda). A high-speed drill (Foredom) with a 0.5 mm drill bit was used to drill a burr hole over the marked site. Virus was loaded into a pulled, glass pipette fitted to a Nanoject II system (Drummond Scientific). The pipette tip was lowered 200 μm from the brain surface and allowed to rest for 5 min. 9.2 nLs of virus was injected every 15 s for 25 min for a total volume of 920 nLs. Following injection, the pipette tip remained in position for 5 min before carefully being withdrawn. The injection site was then sealed with a small drop of Vetbond (3M), and the scalp sewn up using vicryl sutures (Ethicon). Animals were allowed to recover on a heating pad and given a post-surgery injection of carprofen subcutaneously to control pain, and up to 3 days following surgery. Injected mice were housed with gender-matched siblings following surgery. Imaging took place 14 days following injection.

Immunohistochemistry

To confirm effective knock out of Arc using AAV5-hSyn-mCherry-Cre, Arc cKO mice were injected at P60 and sacrificed at P74, then perfused with PBS followed by 4% ice-cold paraformaldehyde in PBS. The brain was removed and stored in 4% paraformaldehyde in PBS at 4°C for 24h before being transferred to 30% sucrose in PBS at 4°C until saturated. The brain was cut into 40 μm sections on a Leica 1950 CM cryostat and stored in PBS at 4°C. Sections containing binocular V1 were blocked in 5% normal donkey serum (Jackson ImmunoResearch) and 0.1% Triton X-100 (Amresco) in PBS for 1 h and then transferred into 1:1000 rabbit anti-Arc antibody (Proteintech) diluted in blocking buffer overnight. Sections were then washed 3 times for 10 min each time in PBS, before being placed in secondary donkey anti-rabbit Alexa Fluor 488 (Jackson ImmunoResearch) for 4 h. Sections were then washed 3 times for 10 min each time in PBS before mounting on slides with ProlongGold Antifade reagent (Invitrogen).

Retinotopic mapping

We conducted chronic retinotopic mapping in awake Thy1 GCaMP6s mice at P14 and P20. Calcium responses excited by an X-cite Series 120 Q were captured on a PCO Panda 4.2 sCMOS camera using a tandem lens set up with a 50 mm lens (Computar) and effective magnification of 3.6X. Excitation and emission wavelengths were filtered using a single-band filter set for EGFP (49002, Chroma Technology). Mice were held stationary in a plastic tube, and visual stimuli were presented on an LCD monitor centered perpendicular to the mouse's midline, 36.2 cm from the mouse's head. The monitor covered a field of view 30° in vertical and 70° in horizontal. As the mouse binocular visual field is measured at 40° of the central visual field (Scholl et al., 2017), the majority of the stimulated region was binocular V1 with 15° at the contralateral edge of the monitor exciting monocular V1. After the mouse was placed into the frame, we took an image of the surface vasculature for future alignment and then moved the focal plane 400 μm below the brain surface. Stimulation consisted of a 9° wide white bar moving on a black background continuously and periodically at 9° per second generated by the MATLAB (Mathworks) toolbox, Psychtoolbox. Neither eye was blocked during the recording. The bar drifted across the monitor 40 times in each of the cardinal directions. Frames were captured at 5 Hz with 4x4 binning, except in one scan where the frame rate was set to 10 Hz. Illumination intensity and exposure time were manually set to almost fill the available well depth (Zhuang et al., 2017). After imaging, mice were housed with their dams and reimaged using the

same methods and analysis at P20. Imaging sessions were aligned by the visible window boundaries and the pattern of the vasculature.

Two-photon calcium imaging

Calcium responses were recorded using a raster-scanning two-photon microscope (Bruker Ultima) controlled by Prairie View software. A Coherent Chameleon Ti:Sapphire laser was used for fluorophore excitation, fixed at 920 nm for GCaMP6s imaging, and 1020 nm for mCherry imaging. Laser power was set at 80 mW at the sample. A 20x water immersion objective (Olympus, 1 numerical aperture) was used in all experiments. Images were acquired at 2.64-2.94 Hz over a field of view 594x594 μm at 2.32 μm/pixel. All imaging was performed at a depth of 150-210 μm below the pia as measured from the center of the field of view. We positioned the field of view 1 mm anterior of the rear of the window aligned horizontally to the window's midline. All testing was done in awake, head-fixed mice held stationary in a plastic tube. Mice were anesthetized with 2% isoflurane and placed below the objective and allowed to habituate for 30 min before imaging. Normally reared and dark reared mice did not have their monitor turned on until 5 min before recording. Visual stimuli were presented on an LCD monitor centered perpendicular to the mouse's midline, 36.2 cm from the mouse's head. The monitor covered a field of view 30° in vertical and 70° in horizontal. Visual stimuli consisted of drifting, sinusoidal grating of spatial frequency 0.05 cycles/degree moving 1 cycle/second generated by the MATLAB (Mathworks) toolbox, Psychtoolbox. In one additional group, spatial frequencies of 0.025, 0.05, 0.1, 0.2, and 0.4 cycles/degree were used. Six orientations from 0-150°, each with two directions of movement orthogonal to their orientation, were used to elicit calcium responses. Each direction was repeated 5 times in pseudorandom order. Visual stimuli were each presented for 5 s with 5 s of a gray screen between each presentation. Visual stimuli were time-locked to data acquisition using a 5-V square wave pulse generated using a Measurement Computing USB-1208FS-Plus data acquisition board and recorded by Prairie View. Visual stimuli were presented independently to the contralateral or ipsilateral eye by placing an opaque eye block in front of the opposing eye to temporarily occlude vision. The eye stimulated first (contralateral or ipsilateral) was randomized between animals and recordings.

QUANTIFICATION AND STATISTICAL ANALYSIS

Analysis of retinotopy data

We analyzed captured images for each direction using previously describe methods to extract the frequency component corresponding to the repetition rate of the stimulus (Kalatsky and Stryker, 2003; McCurry et al., 2010; Zhuang et al., 2017). Briefly, we first removed the slow noise component using a high pass temporal filter (twice the repetition rate), converted the frames to ΔF/F using the mean of a 10 s period with no stimulation, computed the mean response and took the first harmonic frequency of the Fourier transform for each pixel (Ramesh et al., 2018). The map of altitude was computed using the two trials with stimuli moving in opposing vertical directions to remove delay between stimulus and response arising from indicator kinetics (Zhuang et al., 2017). The magnitude was computed using the sum of all 4 directions (Ramesh et al., 2018). We defined V1 as the pixels with magnitude within 40% of the maximum magnitude (McCurry et al., 2010).

Analysis of two-photon imaging data

Only one FOV was quantified for each animal. Collected frames were opened in ImageJ (NIH) using the Prairie Reader plugin, and contralateral and ipsilateral recordings concatenated. The two-photon calcium imaging analysis pipeline, Suite2P (https://github.com/MouseLand/suite2p) was used to register and detect cells in recorded data. Default settings for the December 2018 distribution of Suite2P were used with the exception of the following: diameter of 9, Tau of 2, frames per second 2.64 or 2.94, 3 neuropil to cell ratio, and 191 minimum neuropil pixels. Detected ROIs were manually curated to discard ROIs in which a neuronal somatic ROI was not visible in the mean image. Remaining ROIs were classified as putative neurons active during the recording period. All further analysis was carried out using custom functions written in MATLAB (https://github.com/Shepherdlab/2Photon). To compare baseline fluorescence in WT and Arc KO mice across age, we took the 5th percentile of fluorescence during the interstimulus interval. We measured spontaneous activity using the ΔF/F ($(F-F_0)/F_0$, neuropil correction factor set to 0.7 (Stringer et al., 2019)) trace from the contralateral eye by measuring the area under the curve of events above 0.1 ΔF/F during the blank screen period, excluding the first second to avoid residual decay from the preceding stimulus (as analyzed previously, Keck et al., 2013). Due to the high neuropil signal in the densely labeled Thy1 GCaMP6s line, mean F_0 after neuropil subtraction can, in some cases, be close to 0, leading to misleading fold changes in fluorescence. Therefore, we used Z-scores ($(F-F_0)/F_{STD}$), which report the change in fluorescence (ΔF) normalized to the variance in baseline (standard deviation of gray screen period) rather than the mean fluorescence of baseline (mean of F_0) for all other comparisons (El-Boustani et al., 2018).

Following Z-scoring, the periods preceding and including the five presentations of each unique stimulus weresegmented. The means of each presentation and its corresponding pre-stimulus period were statistically compared using a paired sample t test (MATLAB). The 5 stimulus presentations were then averaged together as a robust mean, and the mean Z-score of the mean trace during the stimulus calculated. Only neurons with a significant response to at least one stimulus (during stimulation of either the contralateral or ipsilateral eye) were included in further analysis. The criteria used to determine a significant response was a p value of the paired t test below 0.05, and a mean Z-score above 0.5 for the same unique stimulus. This amplitude threshold was determined by taking the 99.58th percentile of mean responses during gray screen (no stimulus periods) for all ages. To determine the false

discovery rate of this method, we used random timestamps from the recording in place of the timestamps of stimulus onset for P14, P20, and P30 WT mice. Mean false discovery for each eye was 1.0% for P14, 2.3% for P20, and 1.2% for P30. Mean total false discovery (contralateral+ipsilateral) for each age group is 1.9% for P14, 4.5% for P20, and 2.4% for P30. A ratio of the number of neurons responding to the contralateral eye and the number of neurons responding to the ipsilateral eye was calculated for each mouse. Within each group (genotype/age), this measure was used to remove outliers more than 1 standard deviation from the mean of the group prior to the analysis below. The probability of a neuron being binocular was calculated as

$$\text{Binocular probability} = \left(\frac{\textit{contralateral responses}}{\textit{total responses}}\right) * \left(\frac{\textit{ipsilateral responses}}{\textit{total responses}}\right)$$

Responsive neurons were classified based on whether there was a significant response to stimulation of both the contralateral and ipsilateral eye (binocular), or only to one eye (contralateral or ipsilateral). For all responsive neurons, their direction selectivity was calculated using a global measure of direction selectivity equal to

$$\text{DSI} = \frac{abs\left(\left(\sum_k R(\theta k)\exp(i\theta k)\right)\right)}{\sum_k R(\theta k)}$$

Where R(θk) is the response to the direction θk. Orientation selectivity was calculated in a similar manner, where

$$\text{OSI} = \frac{abs\left(\left(\sum_k R(\theta k)\exp(2i\theta k)\right)\right)}{\sum_k R(\theta k)}$$

Where R(θk) is the response to the orientation θk. Orientation preference is derived during the above equation as $abs((\sum_k R(\theta k)\exp(2i\theta k))$, and converted from radians to degrees. The horizontal bias index was calculated for each neuron (or eye-specific response for binocular neurons) as $1 - \min(abs(\textit{orientation preference} - 0^\circ), abs(180^\circ - (\textit{orientation preference} - 0^\circ)))/45^\circ$. The binocular ocular dominance index (ODI), taken as a ratio of their ipsilateral response over the sum of their ipsilateral and contralateral response for binocular neurons, utilized the mean response to the direction which elicited the largest mean response for each eye. Population ODI used an ODI score of 0 for contralateral monocular neurons and 1 for ipsilateral monocular neurons. All data are first averaged within animal and then between animals in a group (age/genotype).

For analysis of neuropil patches, in each recording, a blood vessel passing perpendicular to the plane of imaging was manually selected, and the mean fluorescent signal of the blood vessel in each frame calculated and subtracted from the trace of each neuropil patch. This subtraction controls for any light contamination related to the visual stimuli and assures the neuropil signal reflects true local calcium fluctuations. Calculation of Z-score and defining significant visual responses were done identically for neuropil and neurons. Signal correlation between the contralateral and ipsilateral responses was calculated as a linear Pearson correlation between vectors of the mean response to each direction in MATLAB (Jeon et al., 2018; Ko et al., 2013).

n in all statistics listed in the results is the number of animals. The number of neurons is not used as statistical n for any comparison between groups in this study to avoid bias from biological replicates. No test was used prior to the study to determine sample size, and the distributions were not tested for normalcy. In all plots, we display the mean and SEM of each group as well as the individual data points for animals within the group. Calculation of paired t test between pre and post-stimulation means on individual trials was calculated using built-in MATLAB functions. All other statistics were calculated using JMP (SAS). The significance level was set at $\alpha < 0.05$ for all within/two group comparisons using a two-sample ANOVA or t test. Otherwise, an ANOVA was used to calculate an F value and p value followed by a post hoc Tukey's Honest Significant Difference test to determine significant differences between groups. F and t statistics are reported for all comparisons in the results.

DATA AND CODE AVAILABILITY

The code generated during this study is available at https://github.com/Shepherdlab/2Photon. The raw imaging data are available upon request.

Cell Reports, Volume *30*

Supplemental Information

Experience-Dependent Development and Maintenance of Binocular Neurons in the Mouse Visual Cortex

Kyle R. Jenks and Jason D. Shepherd

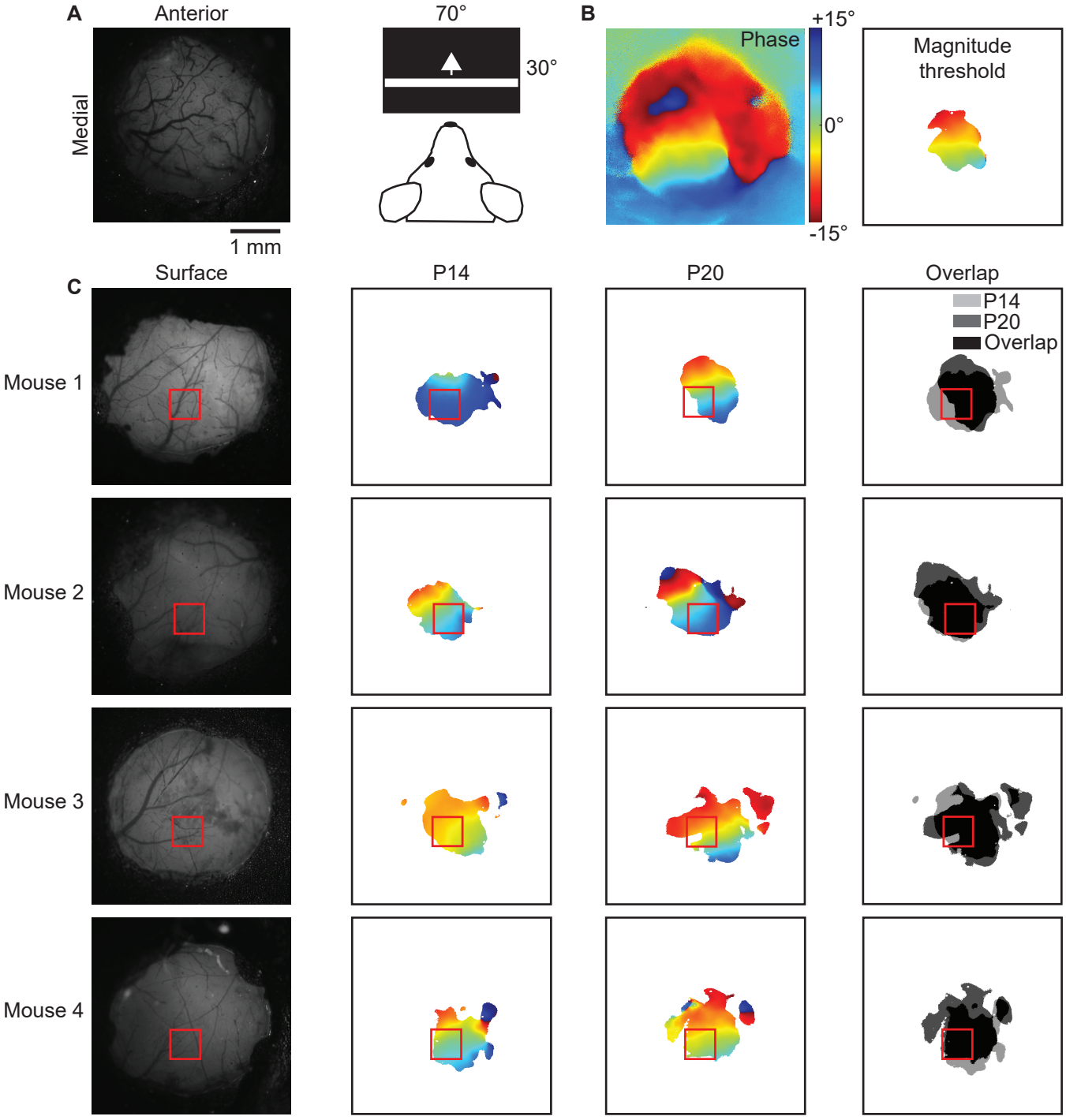
A
Anterior
Medial
1 mm
70°
30°
B
Phase
+15°
0°
-15°
Magnitude threshold
C
Surface
P14
P20
Overlap
P14
P20
Overlap
Mouse 1
Mouse 2
Mouse 3
Mouse 4

Figure S1. Retinotopic mapping of V1 in P14 mice. Related to Figure 1. A. *Retinotopic mapping protocol*. An example image of the brain surface imaged through a cranial window (left). During imaging, mice viewed (both eyes open) a drifting periodic stimulus of a white, 9° bar drifting periodically on a black background in the 4 cardinal directions on a monitor covering 30° of the vertical visual field and 35° on either side of the midline (right). **B.** *Retinotopic analysis*. Example altitude phase map from a P40 mouse shows a retinotopic gradient corresponding to a range from -15 to +15° of the visual field (left). This phase map is thresholded by the magnitude of the response at the visual stimulus frequency to define V1, which has a larger magnitude visual response than surrounding brain regions (right). **C.** *Chronic retinotopic imaging*. Four P14 mice were imaged at P14 and then again at P20. Each row represents an individual mouse. The surface image shows the pattern of the brain vasculature and edges of the window. The red box shows where images would be taken for a two-photon imaging experiment based solely on stereotaxic coordinates and corresponds to the size of the field of view. The P14 image shows the thresholded altitude map from the P14 recording. The P20 image shows the thresholded altitude map from the same mouse at P20. The overlap image shows the area of the P14 map (light grey), P20 map (dark grey), and overlap of the P14 and P20 map (black).

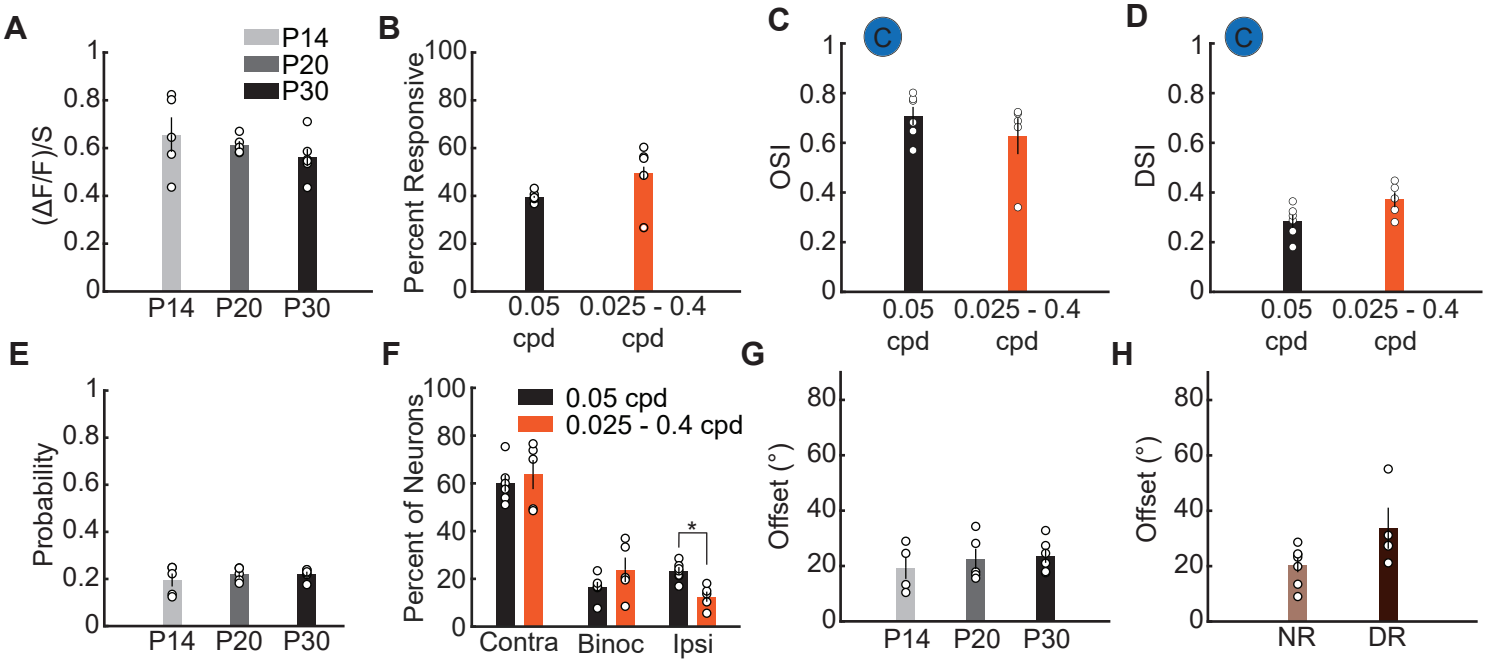
A
P14
P20
P30
(ΔF/F)/S
1
0.8
0.6
0.4
0.2
0
P14 P20 P30
B
Percent Responsive
100
80
60
40
20
0
0.05 cpd
0.025 - 0.4 cpd
C
C
OSI
1
0.8
0.6
0.4
0.2
0
0.05 cpd
0.025 - 0.4 cpd
D
C
DSI
1
0.8
0.6
0.4
0.2
0
0.05 cpd
0.025 - 0.4 cpd
E
Probability
1
0.8
0.6
0.4
0.2
0
P14 P20 P30
F
Percent of Neurons
0.05 cpd
0.025 - 0.4 cpd
100
80
60
40
20
0
*
Contra
Binoc
Ipsi
G
Offset (°)
80
60
40
20
0
P14 P20 P30
H
Offset (°)
80
60
40
20
0
NR
DR

Figure S2. Development of binocular responses and binocular matching in the visual cortex. Related to Figures 1 and 2. A. Measure of spontaneous activity during the interstimulus interval determined as the area under the curve of the ΔF/F trace over time. **B.** Comparison of the percentage of total neurons detected at P30 that respond significantly to a visual stimulus using either a single (0.05 cycles/degree, cpd) or multiple (0.025, 0.5, 0.1, 0.2, and 0.4 cpd) spatial frequencies. **C.** Comparison of binocular contralateral OSI using either a single (0.05 cycles/degree, cpd) or multiple (0.025, 0.5, 0.1, 0.2, and 0.4 cpd) spatial frequencies. **D.** Comparison of binocular contralateral DSI using either a single (0.05 cycles/degree, cpd) or multiple (0.025, 0.5, 0.1, 0.2, and 0.4 cpd) spatial frequencies. **E.** Theoretical probability of a visually responsive neuron being binocular given the number of contralaterally and ipsilaterally responsive neurons at each age. **F.** Percent of visually responsive neurons that are contralateral, binocular, or ipsilateral responsive at P30 that respond significantly to a visual stimulus using either a single (0.05 cpd) or multiple (0.025, 0.5, 0.1, 0.2, and 0.4 cpd) spatial frequencies. **G.** Average offset in orientation preference of the contralateral and ipsilateral responses in binocular neurons of WT mice over development. **H.** Average binocular offset in normally reared (NR) and dark reared (DR) mice. ($*p < 0.05$ indicates a significant difference between groups. Error bars represent standard error of the mean. Open circles indicate a data point from an individual mouse. n=number of animals for all statistics).

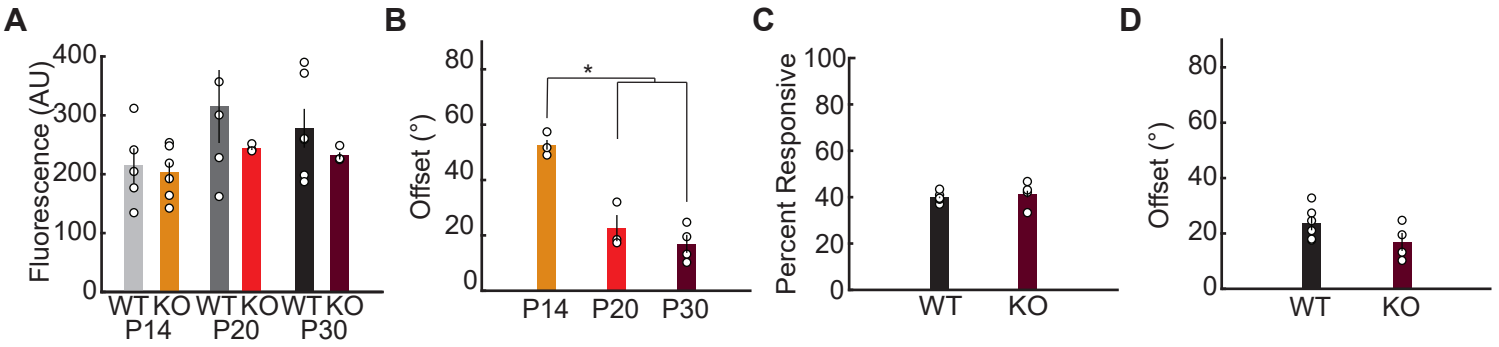
A
Fluorescence (AU)
400
300
200
100
0
WT KO WT KO WT KO
P14 P20 P30
B
Offset (°)
80
60
40
20
0
*
P14 P20 P30
C
Percent Responsive
100
80
60
40
20
0
WT KO
D
Offset (°)
80
60
40
20
0
WT KO

Figure S3. Visual responses in P30 Arc KO mice do not significantly differ from WT mice. Related to Figure 4. A. The lowest 5th percentile of fluorescence during the interstimulus period in WT and Arc KO mice across development, indicating no effect of low GFP expression in the Arc KO line. **B.** Average offset in orientation preference of the contralateral and ipsilateral responses of binocular neurons of Arc KO mice across development. **C.** Percent of visually responsive neurons in P30 WT and Arc KO mice. **D.** Binocular offset of P30 WT and Arc KO binocular neurons. (*$p < 0.05$ indicates a significant difference between groups. Error bars represent standard error of the mean. Open circles indicate a data point from an individual mouse. n=number of animals for all statistics).

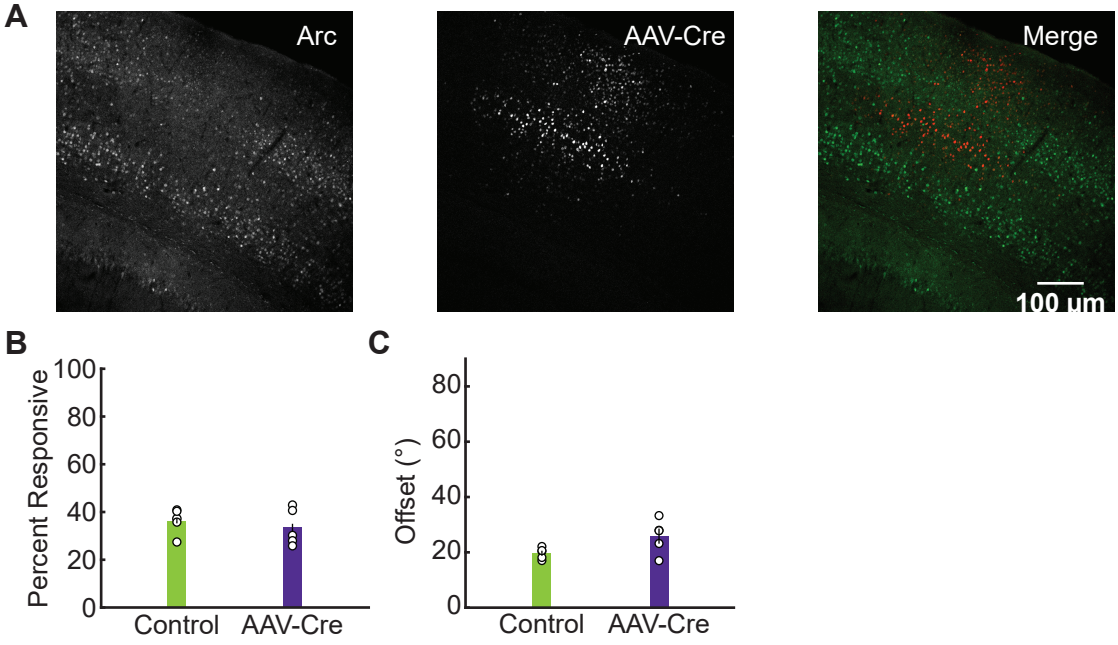
A
Arc
AAV-Cre
Merge
100 µm
B
Percent Responsive
100
80
60
40
20
0
Control
AAV-Cre
C
Offset (°)
80
60
40
20
0
Control
AAV-Cre

Figure S4. Conditional deletion of Arc in binocular V1. Related to Figure 5. A. Representative image of immunohistochemistry performed in an AAV-Cre-mCherry injected Arc cKO mouse. Arc protein staining (green, left panel) is selectively decreased in the region of mCherry expression (red, middle panel. Right panel, merge). **B.** Percent of neurons that are visually responsive in Control and AAV-Cre mice. **C.** Binocular offset in Control and AAV-Cre mice. (Error bars represent standard error of the mean. Open circles indicate a data point from an individual mouse. n=number of animals for all statistics).

Table S1. Visual response properties for all genotypes and ages. Related to Figures 1, 2, 4, and 5. Response properties of all groups used in the main study, separated for monocular (upper) and binocular (lower) cells. Number in parentheses next to each group reports n, number of mice in group. Number listed for response properties reports mean of group ± the standard error of the mean.

Monocular					
Genotype/ Age (n)	**Contra OSI**	**Ipsi OSI**	**Contra DSI**	**Ipsi DSI**	
WT P14 (5)	0.45±0.05	0.61±0.09	0.50±0.03	0.46±0.07	
WT P20 (5)	0.75±0.02	0.60±0.08	0.37±0.03	0.35±0.03	
WT P30 (6)	0.73±0.02	0.70±0.02	0.39±0.02	0.36±0.03	
Arc KO P14 (6)	0.55±0.05	0.48±0.08	0.49±0.02	0.41±0.03	
Arc KO P20 (3)	0.73±0.03	0.56±0.06	0.40±0.02	0.40±0.06	
Arc KO P30 (4)	0.73±0.05	0.67±0.02	0.32±0.05	0.34±0.04	
NR WT (7)	0.75±0.02	0.58±0.04	0.33±0.02	0.35±0.03	
DR WT (4)	0.68±0.05	0.67±0.05	0.60±0.05	0.43±0.04	
Control cKO (5)	0.78±0.01	0.68±0.06	0.37±0.06	0.34±0.05	
AAV-Cre cKO (5)	0.78±0.01	0.68±0.03	0.34±0.03	0.32±0.02	
Binocular					
Genotype/ Age (n)	**Contra OSI**	**Ipsi OSI**	**Contra DSI**	**Ipsi DSI**	**Binocular ODI**
WT P14 (4)	0.44±0.08	0.68±0.12	0.45±0.04	0.45±0.12	0.39±0.08
WT P20 (5)	0.72±0.04	0.75±0.05	0.28±0.04	0.32±0.04	0.45±0.04
WT P30 (6)	0.71±0.04	0.63±0.04	0.28±0.03	0.30±0.02	0.38±0.03
Arc KO P14 (3)	0.46±0.23	0.51±0.22	0.46±0.03	0.56±0.10	0.33±0.07
Arc KO P20 (3)	0.80±0.04	0.76±0.07	0.37±0.05	0.36±0.14	0.38±0.03
Arc KO P30 (4)	0.71±0.05	0.70±0.05	0.23±0.01	0.27±0.01	0.41±0.02
NR WT (7)	0.71±0.05	0.63±0.08	0.23±0.02	0.36±0.03	0.33±0.02
DR WT (4)	0.59±0.08	0.55±0.06	0.39±0.09	0.27±0.02	0.32±0.03
Control cKO (5)	0.81±0.02	0.73±0.01	0.24±0.05	0.26±0.03	0.41±0.02
AAV-Cre cKO (5)	0.74±0.04	0.66±0.06	0.26±0.02	0.22±0.02	0.35±0.03